Vancomycin-decorated microbubbles as a theranostic agent for Staphylococcus aureus biofilms

Kouijzer, Joop J.P.; Lattwein, Kirby R.; Beekers, Inés; Langeveld, Simone A.G.; Leon-Grooters, Mariël; Strub, Jean Marc; Oliva, Estefania; de Jong, Nico; van der Steen, Antonius F.W.; More Authors

DOI
10.1016/j.ijpharm.2021.121154

Publication date
2021

Document Version
Final published version

Published in
International Journal of Pharmaceutics

International Journal of Pharmaceutics 609 (2021) 121154

Contents lists available at ScienceDirect

International Journal of Pharmaceutics

journal homepage: www.elsevier.com/locate/ijpharm

Vancomycin-decorated microbubbles as a theranostic agent for *Staphylococcus aureus* biofilms

Joop J.P. Kouijzer [a,*], Kirby R. Lattwein [a], Inés Beekers [a], Simone A.G. Langeveld [a], Mariël Leon-Grooters [a], Jean-Marc Strub [b], Estefania Oliva [c], Gaëtan L.A. Mislin [d], Nico de Jong [a,e], Antonius F.W. van der Steen [a,e], Alexander L. Klibanov [f], Willem J. B. van Wamel [g], Klazina Kooiman [a]

[a] Department of Biomedical Engineering, Thoraxcenter, Erasmus MC University Medical Center Rotterdam, Office Ee2302, P.O. Box 2040, 3000 CA Rotterdam, the Netherlands
[b] CNRS/University of Strasbourg UMR 7178, Institut Pluridisciplinaire Hubert Curien, Laboratoire de Spectrométrie de Masse Bio-Organique, 25 rue Becquerel, F-67087 Strasbourg-Cedex 2, France
[c] Faculté de Pharmacie de Strasbourg, Plateforme d'Analyse Chimique de Strasbourg-Illkirch (PACSI), 74 route du Rhin, F-67400 Illkirch-Graffenstaden, France
[d] CNRS/University of Strasbourg UMR7242, 300 Boulevard Sébastien Brant, F-67400 Illkirch-Graffenstaden, France
[e] Laboratory of Acoustical Wavefield Imaging, Faculty of Applied Sciences, Delft University of Technology, Building 22, Room D218, Lorentzweg 1, 2628 CJ Delft, the Netherlands
[f] Cardiovascular Division, Department of Medicine, University of Virginia, UVA CVRC, PO Box 801394, Charlottesville, VA 22908, USA
[g] Department of Medical Microbiology and Infectious Diseases, Erasmus MC, Office Na9182, P.O. Box 2040, 3000 CA Rotterdam, the Netherlands

ARTICLE INFO

Keywords:
Biofilm
Sonobactericide
Targeted microbubble
Theranostic
Ultrasound
Vancomycin

ABSTRACT

Bacterial biofilms are a huge burden on our healthcare systems worldwide. The lack of specificity in diagnostic and treatment possibilities result in difficult-to-treat and persistent infections. The aim of this *in vitro* study was to investigate if microbubbles targeted specifically to bacteria in biofilms could be used both for diagnosis as well for sonobactericide treatment and demonstrate their theranostic potential for biofilm infection management. The antibiotic vancomycin was chemically coupled to the lipid shell of microbubbles and validated using mass spectrometry and high-axial resolution 4Pi confocal microscopy. Theranostic proof-of-principle was investigated by demonstrating the specific binding of vancomycin-decorated microbubbles (vMB) to statically and flow grown *Staphylococcus aureus (S. aureus)* biofilms under increasing shear stress flow conditions (0–12 dyn/cm^2), as well as confirmation of microbubble oscillation and biofilm disruption upon ultrasound exposure (2 MHz, 250 kPa, and 5,000 or 10,000 cycles) during flow shear stress of 5 dyn/cm^2 using time-lapse confocal microscopy combined with the Brandaris 128 ultra-high-speed camera. Vancomycin was successfully incorporated into the microbubble lipid shell. vMB bound significantly more often than control microbubbles to biofilms, also in the presence of free vancomycin (up to 1000 μg/mL) and remained bound under increasing shear stress flow conditions (up to 12 dyn/cm^2). Upon ultrasound insonification biofilm area was reduced of up to 28%, as confirmed by confocal microscopy. Our results confirm the successful production of vMB and support their potential as a new theranostic tool for *S. aureus* biofilm infections by allowing for specific bacterial detection and biofilm disruption.

1. Introduction

Approximately 80% of all bacterial infections are associated with biofilms (Health, 2002), where bacteria encase themselves in a protective matrix hindering antibiotic effectiveness up to 1000-fold compared to free-floating (i.e., planktonic) bacteria and facilitating development of antibiotic resistance (Mah and O'Toole, 2001; Waters et al., 2016). This increased resistance is largely due to the reduced metabolic activity of biofilm-embedded bacteria and the limited penetration of antibiotics throughout the biofilm (Steward and Costerton, 2001; Ito et al., 2009; Lewis, 2005). These life-threatening infections are challenging to diagnose and treat, and are increasing in prevalence alongside the

* Corresponding author.
E-mail address: j.kouijzer@erasmusmc.nl (J.J.P. Kouijzer).

https://doi.org/10.1016/j.ijpharm.2021.121154
Received 22 May 2021; Received in revised form 28 September 2021; Accepted 30 September 2021
Available online 6 October 2021

vulnerable aging population and surging use of implantable life-saving/enhancing technologies that create niches primed for colonization (Cassini et al., 2019; Lee et al., 2021). Furthermore, biofilm infections are difficult to cure, often requiring high-risk, costly, invasive procedures and can still become persistent, necessitating lifelong antibiotic use and/or repeated medical interventions. Biofilm infections can occur anywhere in all organ systems and can carry a high mortality rate depending on the location and infecting microbe. For example, infective endocarditis is an infection of the heart valves and/or endocardial surface with an in-hospital mortality of 18–47.5% (Chirouze et al., 2004; Murdoch, 2009) and a 5-year mortality of 40–69% (Mirabel et al., 2014; Bannay et al., 2011; Bin Abdulhak et al., 2014; Tahon et al., 2021). Delayed diagnosis of infective endocarditis is associated with increased mortality and early diagnosis of biofilm infection is therefore critical (Mirabel et al., 2014; DeSimone and Sohail, 2016; Kreitmann et al., 2020). Currently there is no theranostic tool available in the clinic which combines the detection of biofilms with treatment possibilities. A novel theranostic agent to detect early biofilm formation with subsequent treatment possibilities would be a major breakthrough.

Microbubbles (1–10 μm in diameter) are ultrasound contrast agents that consist of an inert-gas core encapsulated by a protein, phospholipid, or biocompatible polymer shell (Kooiman et al., 2014; Daeichin et al., 2017) and used in daily clinical practice for several decades to aid in the ultrasound diagnosis of cardiovascular diseases and cancer (Kooiman et al., 2014; Kooiman et al., 2020; Sennoga et al., 2017; Schinkel et al., 2020). Their therapeutic potential, however, has only begun being substantiated with clinical trials over the past years (Dimcevski et al., 2016; Kotopoulis et al., 2013; Lipsman et al., 2018; Mainprize et al., 2019). Microbubbles respond volumetrically, i.e., oscillate, to the increase and decrease of pressure from ultrasonic waves (Kooiman et al., 2014; Daeichin et al., 2017), and it is these ultrasound-activated responses that enable them to be detected as well as induce various bioeffects for potential therapeutic applications. Promising pre-clinical investigations have only recently begun to determine if microbubble-mediated effects can be used to treat bacterial infections, which is referred to as sonobactericide (Lattwein et al., 2020). Until now, biofilms both grown and then treated under flow with sonobactericide have yet to be investigated, which would be physiologically relevant for infections situated in flow environments.

Targeted microbubbles are microbubbles that have a ligand incorporated into their coating so they can specifically bind to biomarkers, and have been extensively studied for their theranostic potential in regards to mammalian cells (Kosareva et al., 2020). Preclinically, targeted microbubble binding under flow conditions has been used for the diagnosis of atherosclerosis (Moccetti et al., 2018), while clinical studies have shown the potential of ultrasound molecular imaging of cancer (Willmann et al., 2017; Smeenge et al., 2017). Treatment of different diseases was more effective with targeted than with non-targeted microbubbles in *in vitro* and *in vivo* studies (Kooiman et al., 2020; van Rooij et al., 2015). To the best of our knowledge, targeted microbubbles for biofilms have been investigated only once before, which was for the detection of *Staphylococcus aureus* (*S. aureus*) biofilms using a monoclonal immunoglobulin antibody to protein A (*S. aureus* bacterial cell wall surface protein) or a *Pseudomonas aeruginosa* lectin (Anastasiadis et al., 2014). Although these microbubbles successfully bound to the biofilms, the clinical translation is poor because the antibody to protein A must compete with host antibodies that already bind to protein A for immune surveillance/clearance and the *P. aeruginosa* lectin causes red blood cell agglutination (Gilboa-Garber and Sudakevitz, 1999; Broker et al., 2014).

The purpose of this proof-of-principle study was to develop a clinically translatable novel theranostic agent using vancomycin-decorated microbubbles (vMB) for the detection and treatment of clinically relevant bacteria-associated biofilms. The antibiotic vancomycin was chosen as the ligand for its 1) binding ability to the D-Ala-D-Ala moiety (K_D ~ 1 – 4 μM) present in most Gram-positive bacterial cell walls (Wang et al., 2018), 2) potential for clinical application, and 3) possibility to covalently couple this compound without losing its functionality (Fig. 1) (van Oosten et al., 2013). Vancomycin was chemically coupled to the microbubble coating via the functionalized polyethylene-glycol (PEG) conjugated lipid (DSPE-PEG(3400)) and confirmed with matrix-assisted laser desorption/ionization - time-of-flight mass spectrometry (MALDI-TOF MS), thin-layer chromatography (TLC), and 4Pi microscopy imaging. To mimic physiological conditions, a biofilm flow model was grown and treated under physiological shear stress conditions using an Ibidi microchannel flow set-up. We investigated the capability of the vMB to remain bound to bacterial biofilms under static and shear stress conditions and evaluated their theranostic potential using confocal microscopy combined with ultra-high-speed imaging using the Brandaris 128.

2. Methods

2.1. Conjugation of vancomycin to phospholipid and incorporation in the microbubble shell

2.1.1. Vancomycin coupling to lipid DSPE-PEG(3400)-N-hydroxysuccinimide

Thirty milligrams of DSPE-PEG(3400)-*N*-hydroxysuccinimide (DSPE-PEG(3400)-NHS; Sunbright DSPE-034GS; NOF America Corporation, New York, USA or NOF Europe GmbH, Frankfurt am Main, Germany) was dissolved in 1280 μL dimethylsulfoxide (276855; Sigma-Aldrich, Saint. Louis, Missouri, USA) for a final concentration of 23.4 mg/mL. The covalent coupling of vancomycin to DSPE-PEG(3400)-NHS was performed as previously described for coupling of the cyclic RGD peptide (Unnikrishnan et al., 2019), where the NHS ester of DSPE-PEG reacts with the primary amino group of the peptide. The reaction mixture was made by adding the DSPE-PEG(3400)-NHS solution to a 20% molar excess of vancomycin hydrochloride hydrate (V0045000, Sigma-Aldrich) in dimethylsulfoxide. A 2-fold molar excess of *N,N*-diisopropylethylamine (496219, Sigma-Aldrich) relative to the vancomycin hydrochloride hydrate was also added. The reaction mixture was incubated on a rocker (15 rpm, PTR-35, Grant Instruments Ltd, Shepreth, United Kingdom) overnight at room temperature. *N*-hydroxy succinimide, unreacted vancomycin, and byproducts were removed by dialysis (Spectra/Por 1 Dialysis Membrane 6–8 kD; Spectrum, New Jersey, USA) in 500 mL 0.9% saline solution (Baxter International Inc., Deerfield, Illinois, USA) at 4 °C for 24 h. Then the saline solution was replaced with 4 °C demi water every 24 h for two days. On the fourth day of dialysis, the demi water was replaced twice with 4 h in between to reach the microSiemens value (Greisinger GMH 3431, Regenstauf, Germany) of demi water, i.e. 1–3 μS. The final product (Fig. 1) was then freeze-dried (Alpha 1–2 LD plus; Martin Christ GmbH, Osterode am Harz, Germany) and stored at −20 °C. Depending on the supplier of the DSPE-PEG(3400)-NHS, the produced DSPE-PEG(3400)-vancomycin conjugate is referred to as 'lipid conjugate (batch USA)', i.e. made from the DSPE-PEG(3400)-NHS obtained from NOF America Corporation or 'lipid conjugate (batch EU)', i.e. made from DSPE-PEG(3400)-NHS obtained from NOF Europe.

2.1.2. Mass spectrometry

Electrospray ionization mass spectrometry experiments were performed on an Agilent Accurate Mass QToF 6520 quadrupole time-of-flight instrument (Agilent Technologies, Santa Clara, CA, USA) based on mass spectrometry analysis reported for similar compounds (Dauty et al., 2002). The electrospray ionization source was operated in the positive ionization mode using a capillary voltage of 4500 V and the following conditions: nebulizer nitrogen gas pressure, 10 psig; drying gas flow rate, 5 L/min; and drying temperature, 340 °C. The scan range was m/z 50–3200 at 1 s/scan. Data acquisition was performed using MassHunter Qualitative Analysis software (B.07.00, Agilent). Direct introduction conditions: samples were prepared at a concentration of 1 mg/mL (in chloroform for the DSPE-PEG(3400)-NHS, lipid conjugate

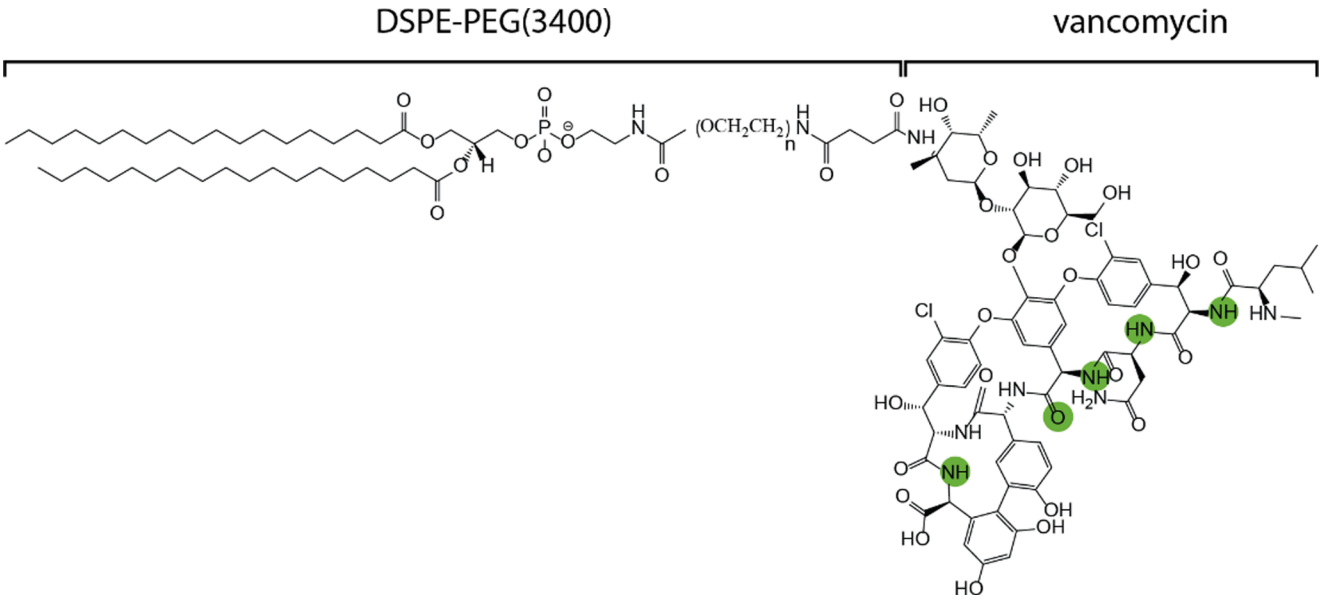

Fig. 1. Molecular structure of the functionalized polyethylene-glycol (PEG) conjugated lipid (DSPE-PEG(3400)) coupled to the antibiotic molecule vancomycin. Green circles indicate where the vancomycin interacts with the D-Ala-D-Ala moiety present in Gram-positive bacterial cell walls (McComas et al., 2003).

(batch USA), and lipid conjugate (batch EU) and in water for vancomycin) and 1 μL was injected. Injections were done using acetonitrile as the mobile phase with a flow rate of 0.1 mL/min. MALDI-TOF Mass measurements were carried out on an AutoflexTM MALDI-TOF mass spectrometer (Bruker Daltonics GmbH, Bremen, Germany). This instrument was used at a maximum accelerating potential of 20 kV in positive mode and was operated in linear mode. The delay extraction was fixed at 560 ns and the frequency of the laser (nitrogen 337 nm) was set at 5 Hz. The acquisition mass range was set to 2,000–8,000 *m/z* with a matrix suppression deflection (cut off) set to 1,500 *m/z*. The equipment was externally calibrated with the single charge and double ion of insulin. Each raw spectrum was opened with flexAnalysis 2.4 build 11 (Bruker Daltonics GmbH, Bremen, Germany) software and processed using the following parameters: Savitzky-Golay algorithm for smoothing (width 5 and cycles 2), and sum algorithm for peak detection and labelling. The matrix solution was prepared from a saturated solution of α-cyano-4-hydroxycinnamic acid in water/acetonitrile 50/50. The sample (<0.1 mg) was suspended in 1 mL of chloroform, and then 1 μL of the sample was added to 10 μL of saturated matrix solution. The mixture (1 μL) was loaded on the target and dried at room temperature.

2.1.3. Thin-layer chromatography

TLC sheets (TLC Silica gel 60 F_{254} Aluminum sheets; EMD Millipore Corporation, Burlington, Massachusetts, USA) were used as a stationary phase. A mixture of chloroform and methanol in a 9:1 v/v ratio was used as the mobile phase. DSPE-PEG(3400)-NHS and the lipid conjugate (batch USA and EU), were dissolved in chloroform to a concentration of 25 mg/mL and vancomycin was dissolved in methanol to a concentration of 25 mg/mL. Dissolved compounds were then spotted onto the TLC sheet using glass capillaries. Sheets were inspected for compounds under UV light (VL-6 M, Vilber Lourmat, Collégien, France) after exposure to iodine vapors (207772; Thermo Fisher Scientific, Waltham, Massachusetts, USA).

2.1.4. Microbubble production

To produce vMB, 1,2-distearoyl-*sn*-glycero-3-phosphocholine (DSPC, 12.5 mg/mL, 86.4 mol%; Sigma-Aldrich), custom-made lipid conjugate (batch USA or EU) (4.35 mg dissolved as 2.9 mg/mL, 5.3 mol%), and PEG-40 stearate (12.5 mg/mL, 8.3 mol%; Sigma-Aldrich) were first dissolved in phosphate buffered saline (PBS; 14200083; Thermo Fisher Scientific) saturated with perfluorobutane (C_4F_{10}; 355–25-9, F2 Chemicals Ltd, Preston, Lancashire, UK) using a sonicator bath for 10 min. To fluorescently label the vMB coating, the lipid dye DiD (1,1′-dioctadecyl-3,3,3′,3′-tetramethylindodicarbocyanine perchlorate; D307; Thermo Fisher Scientific) was added and mixed by probe sonication (Sonicator Ultrasonic Processor XL2020, Heat Systems, Farmingdale, New York, USA) at 20 kHz at power level 3 for 3 min. This was followed by probe sonication for 60 s at power level 8 under continuous C_4F_{10} gas flow (Klibanov et al., 2004). vMB were produced without the addition of lipid dye for ultrasound molecular imaging experiments and determining the vancomycin concentration on vMB. Microbubbles were stored in sealed 30 mL glass vials (DWK Life Sciences GmbH, Mainz, Germany) under C_4F_{10} atmosphere at 4 °C and used within three days. To produce non-targeted control microbubbles (cMB), the custom-made lipid conjugate was substituted for DSPE-PEG(3400) (2142-3400; Nanosoft Polymers, New York, USA). To fluorescently label the cMB coating, the lipid dye DiD or DiI (1,1′-Dioctadecyl-3,3,3′,3′-tetramethylindocarbocyanine perchlorate; D282; Thermo Fisher Scientific) was added before probe sonication. Before experiments, microbubbles were washed three times with C_4F_{10}-saturated PBS by centrifugation at 400 *g* for 1 min (Heraeus Biofuge Primo, Waltham, Massachusetts, USA). The microbubble size distributions and concentrations were measured using a Coulter Counter Multisizer 3 (Beckman Coulter, Brea, California, USA). Particles (1–30 μm) were quantified using a 50 μm aperture tube. To determine the vancomycin loading efficiency of the vMB, 1970 μL out of a total of 3260 μL washed vMB (batch EU), were sonicated in a water bath for 10 min to destroy the microbubbles. This was followed by freeze-drying (Martin Christ GmbH) which yielded 23.24 mg of destroyed freeze-dried vMB. The destroyed freeze-dried vMB (4.65 and 3.83 mg) and corresponding lipid conjugate (batch EU; 0.79 and 0.48 mg) were dissolved in 50 μL and 350 μL Multi-Assay Manual Diluent (7D82P; Abbott Laboratories, Chicago, Illinois, USA), respectively. The obtained solutions were inserted in the Architect c4000 clinical chemistry analyzer (Abbott Laboratories) in combination with the Multigent vancomycin reagents kit (6E44-21; Abbott Laboratories) to obtain the vancomycin concentration. The vMB loading efficiency was defined by the following formula:

$$\text{Loading efficiency} = \frac{\text{vancomycin in 1 washed vMB batch}}{\text{vancomycin in 4.35 mg lipid conjugate}} \text{x} 100\%$$

The amount of vancomycin molecules per μm^2 of microbubble shell was calculated by dividing the amount of vancomycin on the vMB by the

surface of the vMB: $4\pi N\sum_{i=1}^{k} x_i r_i^2$,where x_i is the number fraction, r_i the radius of that fraction, and k the number of bins (as determined with the Coulter Counter).

2.1.5. 4Pi microscopy imaging

vMB (lipid conjugate batch EU) and DiI-containing cMB were incubated with anti-vancomycin IgG rabbit antibody coupled to a FITC-molecule (1 μg/1 × 10^8 MBs; LS-C540056; LifeSpan BioSciences, Seattle, Washington, USA) on ice for 30 min. To remove excess antibody, microbubbles were washed with C_4F_{10}-saturated PBS as described under 2.1.4. Microbubbles were then placed in 87% glycerol (v/v in PBS) to reduce Brownian motion. Y-stacked xz-scans were acquired using a Leica TCS 4Pi confocal laser-scanning microscope with two aligned opposing objectives for high axial resolution (90 nm step size, 100 × glycerol HCX PL APO objective lens, numerical aperture 1.35). The FITC antibody was excited using a 488 nm laser and detected at 500–550 nm. For lipid shell visualization, DiI and DiD were excited with a 561 nm laser and detected at 580–640 nm and 647–703 nm, respectively. The 'voltex' function in AMIRA software (Version 2020.1, FEI, Mérignac Cedex, France) was used for rendering volume projections of the acquired y-stacked xz-scans.

2.2. Biofilm formation

2.2.1. Static biofilm formation

An infective endocarditis patient-derived *S. aureus* bacterial strain, associated with cardiovascular infections (ST398), was used for this study. This strain was collected by the department of Medical Microbiology and Infectious Diseases, Erasmus MC University Medical Center Rotterdam, the Netherlands, and anonymized and de-identified according to institutional policy. Frozen stock samples were streaked onto tryptic soy agar containing 5% sheep blood (BD, Trypticase™, Thermo Fisher Scientific) and allowed to grow overnight at 37 °C. Bacterial colonies were suspended in Iscove's Modified Dulbecco's Media (IMDM; Gibco, Thermo Fisher Scientific) until an optical density of 0.5 (±0.05) was reached at 600 nm (Ultraspec 10, Amersham Biosciences, Little Chalfont, United Kingdom) corresponding to 1 × 10^8 colony forming units per mL (CFU/mL). IbiTreat polymer μ-Slides (80196; 0.8 mm channel height; I Luer; Ibidi GmbH, Gräfelfing, Germany) were inoculated with 200 μL of diluted bacterial suspension consisting of 1 × 10^4 CFU/mL. The IbiTreat μ-Slide in- and outlet-reservoirs were filled with 60 μL of IMDM. μ-Slides were then incubated at 37 °C for 24 h in a humidified incubator under constant agitation (150 rpm; Rotamax 120, Heidolph Instruments, Schwabach, Germany).

2.2.2. Biofilm formation under flow

IbiTreat μ-Slides were incubated with 320 μL of type O human plasma (citrate phosphate double dextrose as an anti-coagulant; pooled from five donors to minimize donor variability; Sanquin, Rotterdam, the Netherlands) to aid bacterial attachment under flow. After incubation at 37 °C for 24 h in a humidified incubator, plasma was removed and the slides were rinsed three times with 200 μL 0.9% saline solution (Baxter International). Then, an IMDM diluted *S. aureus* bacterial suspension of 200 μL containing 1 × 10^6 CFU/mL was pipetted into the μ-Slide. Bacteria were allowed to attach to the surface of the μ-Slide for 3 h at 37 °C and then the μ-Slide was connected to an Ibidi fluidic unit using corresponding perfusion sets (Perfusion set red, 10962; Ibidi) and a computer-controlled air pressure pump (Ibidi pump system; Ibidi). In order to later on inject microbubbles and dyes, an in-line Luer injection port (10820; Ibidi) was placed in the perfusion set 3.5 cm before the μ-Slide inlet. Biofilms were grown under laminar flow at 5 dyn/cm^2 (14.4 mL/min, corresponding to a Reynolds number of 32) for 24 h at 37 °C.

2.3. Experimental set-up

The μ-Slides were inserted into a custom-built water tank, that was maintained at 37 °C and situated underneath a custom-built Nikon A1R + confocal microscope (Beekers et al., 2019) (Nikon Instruments, Amsterdam, the Netherlands) (Fig. 2A, C). The orientation of the μ-Slide was either upright (Fig. 2A-B) or flipped 180° (Fig. 2C-D) depending on the experiment performed. The transducer (2.25 MHz center frequency used at 2 MHz; 76.2 mm focal length; −6 dB beam width of 3 mm at 2 MHz; V305; Panametrics-NDT, Olympus, Waltham, MA, USA) was placed underneath the sample at a 45° angle to minimize ultrasound reflection and standing wave formation. Both the optical and ultrasound foci were aligned using a pulse-echo approach and a needle tip located at the optical focal plane (Chen et al., 2013), hereby the microbubbles and biofilm could both be simultaneously imaged and insonified. An arbitrary waveform generator (33220A; Agilent), in combination with a broadband amplifier (ENI A-500; Electronics & Innovation, Rochester, NY, USA), was connected to the transducer. The transducer output was calibrated in a separate experiment using a needle hydrophone (1 mm diameter; PA2293; Precision Acoustics, Dorchester, UK). As a live/dead staining, SYTO 9 (S34854; Thermo Fisher Scientific) was excited at 488 nm and detected at 525/50 nm (center wavelength/bandwidth) and propidium iodide (PI; P4864-10ML; Sigma-Aldrich) was excited at 561 nm and detected at 595/50 nm. For experiments with DiI incorporated into the cMB, the 561 nm laser with the same detection was also used for optical imaging. A third channel was used for the visualization of DiD incorporated into vMB or cMB with an excitation at 640 nm and fluorescence detected at 700/75 nm.

2.4. Binding of targeted microbubbles to bacteria in biofilms

2.4.1. Competitive microbubble binding assay

To study the competitive binding of vMB (lipid conjugate batch USA and EU), statically grown biofilms were pre-incubated at room temperature for 5 min with vancomycin concentrations of 0, 10, 20, 100 or 1,000 μg/mL dissolved in IMDM. This includes the maximal recommended clinical blood level concentration of vancomycin, i.e., 20 μg/mL (Pritchard et al., 2010; Tongsai and Koomanachai, 2016). A final vancomycin concentration of 0 or 1,000 μg/mL was used in the μ-Slides for cMB. After this, the dyes (0.4 μL of 5 mM SYTO 9, 5 μL of 1.5 mM PI) and fluorescent DiD microbubbles (7.0 × 10^5 vMB or cMB) were added to IMDM containing the same pre-incubation vancomycin concentration to a total of 200 μL, which was then added to the μ-Slide replacing the pre-incubation. μ-Slides were flipped 180° for 5 min to allow the microbubbles to float up towards the biofilm for binding at room temperature and then flipped back to their original position, such that any unbound microbubbles would rise to the top of the channel (Fig. 2B). For each vancomycin concentration, the binding assay was performed in at least three μ-Slides. μ-Slides were systematically imaged with a 100 × water-dipping objective (CFI Plan 100XC W, Nikon Instruments) of which each field-of-view consisted of 512 × 512 pixels (128 × 128 μm^2). Locations within the μ-Slide were named 1 – 5 and were equally spaced apart, with 1 representing the field-of view nearest to the inlet and 5 nearest to the outlet. The number of microbubbles attached to bacterial biofilms was manually determined using Fiji software for 20 different fields-of-view (5 locations distributed over the length of the microchannel, with 4 equally spaced fields-of-view per location) distributed over each μ-Slide.

2.4.2. Non-specific microbubble binding assay

For assessment of non-specific binding of microbubbles, μ-Slides with and without statically grown biofilms were treated similarly. μ-Slides without biofilm were filled with 200 μL IMDM and in- and outlet-reservoirs with 60 μL of IMDM. μ-Slides were then incubated at 37 °C for 24 h in a humidified incubator under constant agitation (150 rpm). Before the binding assay, all μ-Slides were first rinsed by adding 200 μL IMDM to the inlet and removing 200 μL IMDM from the outlet.

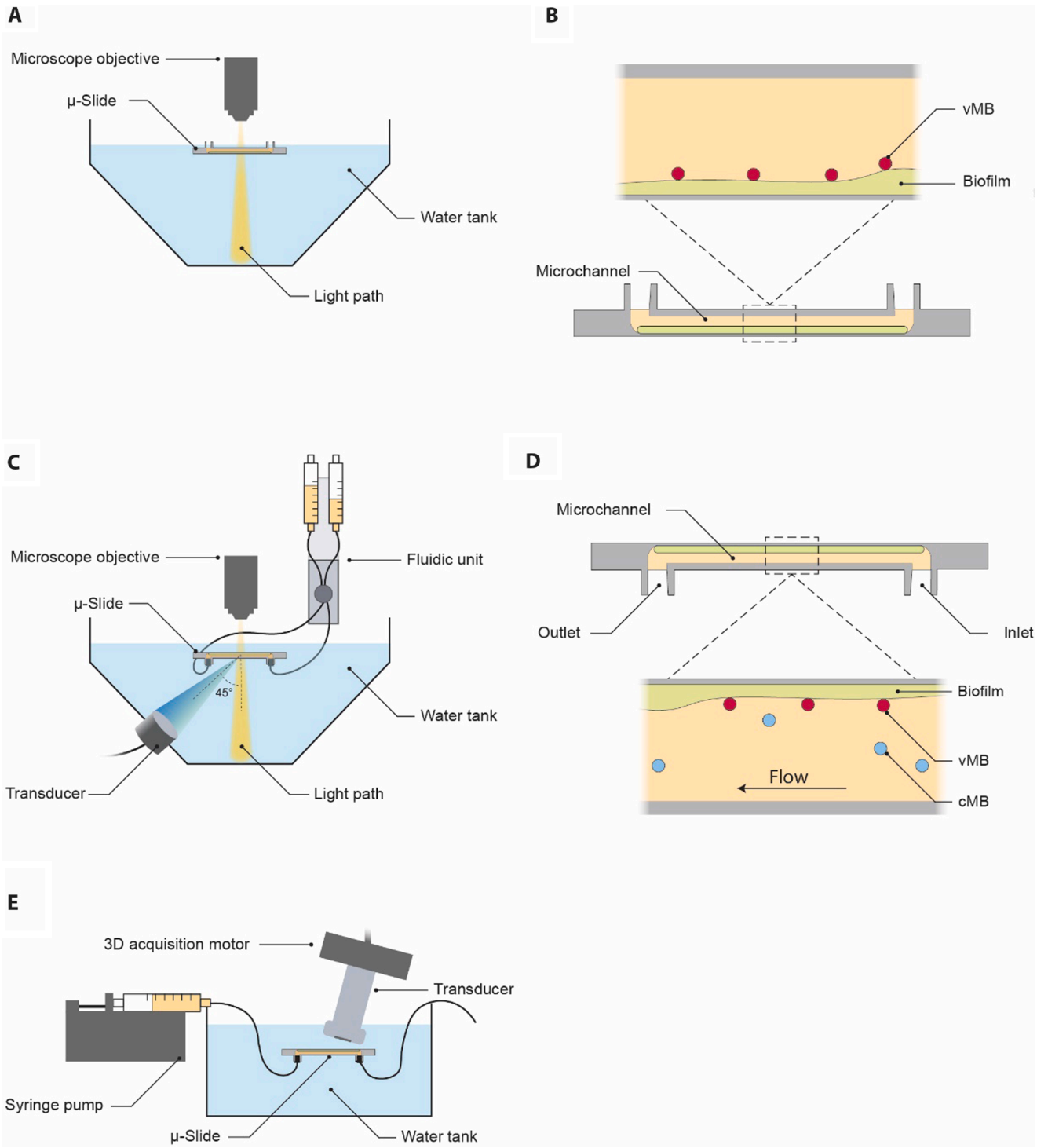

Fig. 2. Schematic representation (not drawn-to-scale) of the experimental set-ups for (A, B) the static experiments, (C, D) the flow experiments and (E) the ultrasound molecular imaging experiment. (B) Zoomed-in cross-section of the Ibidi μ-Slide in A and (D) zoomed-in cross-section of the μ-Slide in C, both indicating the placement of the biofilm within the microchannel containing vancomycin-decorated microbubbles (vMB, red) and control microbubbles (cMB, blue).

After 5 min, 200 μL IMDM containing the dyes (0.4 μL of 5 mM SYTO 9, 5 μL of 1.5 mM PI), 7.0×10^5 fluorescent microbubbles (vMB lipid conjugate batch EU), and either 0, 0.1, or 1% of bovine serum albumin (BSA; A9418-50G; Sigma-Aldrich) (Langeveld et al., 2021; Kooiman et al., 2017) or casein (37582; Thermo Fisher Scientific) (Rychak et al., 2005) was added to the microchannel. μ-Slides were then flipped 180° for 5 min to allow the microbubbles to float up towards the bottom of the microchannel for binding and then flipped back to their original position. Three binding assays were performed for each condition. μ-Slides were systematically imaged with the 100 × objective (for specifics see Section 2.4.1). The number of vMB attached to the bottom and top of the microchannel was manually determined using Fiji software in 40 different field-of-view distributed over the μ-Slide, divided in 20 fields-of-view located at the bottom and 20 fields-of view located at the top of the microchannel. The binding efficiency was defined by the following formula:

$$\text{Binding efficiency} = \frac{\text{Sum amount MBs bottom}}{\text{total amount MBs bottom and top}} \times 100\%$$

2.4.3. Microbubble binding under increasing shear stress

To exclude differences in results due to biofilm heterogeneity and possible variable biofilm erosion under flow conditions, vMB (lipid conjugate batch EU) and DiI-containig cMB were simultaneously added at a ratio of 1:1 to biofilms grown under flow at 5 dyn/cm^2. A solution of 200 μL IMDM containing 0.4 μL of 5 mM SYTO 9 and 1.2 × 10^7 microbubbles was injected into the in-line Luer injection port with a 1 mL Luer Solo syringe (Omnifix-F, B Braun, Melsungen, Germany) and 19G needle (Sterican, B Braun) while the flow was turned off and the Ibidi μ-Slide was oriented upside down (Fig. 2D). To introduce microbubbles and SYTO 9 into the microchannel, a shear stress of 1.3 dyn/cm^2 (3.74 mL/min) was applied for 17 s. The vMB and cMB were then incubated with the biofilm for 5 min without flow. Flow was started and increased every 60 s, with an initial shear stress increase of 0.5 dyn/cm^2 (1.43 mL/min), from 1.5 (4.33 mL/min) to 2 dyn/cm^2 (5.76 mL/min), and then each subsequent step was increased by 1 dyn/cm^2 (~2.87 mL/min) until 12 dyn/cm^2 (34.53 mL/min, Reynolds number: 74.2) was achieved. The number of microbubbles remaining attached to the biofilm while applying increasing flows was monitored with confocal time-lapse microscopy (0.77 frames per second (fps)) using a 60 × water-immersion objective (Plan Apo 60XA WI, Nikon Instruments) of which each field-of-view consisted of 512 × 512 pixels (210 × 210 μm^2). The binding percentage was defined by the following formula:

$$\text{Binding percentage} = \frac{\text{MBs bound after 60 s shear stress}}{\text{total amount MBs before flow}} \text{x} 100\%$$

2.5. Sonobactericide with vancomycin-decorated microbubbles

2.5.1. Sonobactericide therapy

To biofilms grown under flow at 5 dyn/cm^2, a solution of 200 μL containing 0.4 μL of 5 mM SYTO 9, 5 μL of 1.5 mM PI and 1.2 × 10^7 vMB (lipid conjugate batch EU) in IMDM was added into the in-line Luer injection port as described under 2.2.2. After this, a continuous laminar flow of 5 dyn/cm^2 was applied to the biofilm. For sonobactericide therapy, the clinically used transthoracic echocardiography frequency of 2 MHz was chosen (Kremkau, 2015). Biofilms were insonified with ultrasound after a minimum of 50 s of continuous flow exposure. A single 5,000- or 10,000-cycle burst at 250 kPa peak negative pressure was given, resulting in a treatment time of 2.5 or 5 ms. For the ultrasound only control, a single 10,000-cycle burst at 250 kPa peak negative pressure was given. The spatial peak intensity (I_{SP}) was calculated by using the formula: $I_{SP} = P^2/2\rho c$ (Merritt et al., 1992; Kinsler, et al., 2000) where P denotes the peak pressure, ρ denotes the density and c the speed of sound, resulting in a I_{SP} of 2.06 W/cm^2. All experiments were monitored for bacterial and vMB responses with time-lapse confocal microscopy (0.77 fps) using the 60 × objective (for specifics see subsection *2.4.3*).

The biofilm reduction was quantified based on the SYTO 9 signal using a custom-built image analysis code in MATLAB (The MathWorks, Natick, MA, USA). The area without biofilm was determined in a frame before and within 15 s after ultrasound insonification, both selected based on minimal signal variability due to focus drift. Images were first converted to binary by thresholding at 300 (image intensity ranging from 0 to 4095). Next, all connected components were identified through the *bwconncomp* function in MATLAB. All connected components with an area larger than 200 pixels (33.5 μm^2) were classified as areas without biofilm and normalized to the size of the field-of-view (512 × 512 pixels; 210 × 210 μm^2). The biofilm reduction was defined as the change in normalized area without biofilm before and after ultrasound insonification.

2.5.2. Brandaris 128 ultra-high-speed recordings

To resolve the oscillation behavior of the vMB (lipid conjugate batch EU) while bound to the bacterial biofilm under flow at 5 dyn/cm^2 upon ultrasound exposure, the Brandaris 128 ultra-high-speed camera was used as previously described (Beekers et al., 2019). Briefly, the Brandaris 128 was coupled to the custom-built Nikon A1R + confocal microscope, which made it possible to visualize both the microbubble behavior on a microsecond time-scale and sonobactericide treatment effect after ultrasound exposure with high resolution confocal microscopy. Time-lapse confocal imaging using the 100 × objective (for specifics see subsection *2.4.1*) started during continuous flow (5 dyn/cm^2), capturing first the initial state of the biofilm and bound vMB. For the Brandaris 128 ultra-high-speed camera recording, the light path was automatically switched from the confocal scan head to the Brandaris 128 and was defined as t = 0 s. During ultrasound exposure (2 MHz, 250 kPa, 5,000 cycles), the first ~ 14 microbubble oscillations were recorded in 128 frames at a framerate of 14.9 million fps. The microbubble diameter as a function of time was subtracted from the Brandaris 128 recording using custom-designed software (van der Meer et al., 2007). After obtaining all 128 frames, the light path was automatically switched back to the original position to continue confocal time-lapse imaging. The biofilm reduction was quantified as described under 2.5.1 with the exception that 544 pixels were taken for all connected components with an area larger than 33.5 μm^2 to account for the difference in magnification.

2.6. Ultrasound molecular imaging

A high frequency pre-clinical scanner (Vevo 3100, FUJIFILM VisualSonics, Toronto, Canada) was used in combination with an ultra-high frequency linear array transducer (MX250, FUJIFILM VisualSonics) operated at 18 MHz to visualize vMB bound to the biofilm. Biofilms were grown under flow at 5 dyn/cm^2 as described under 2.2.2. with the exception that the perfusion set was modified with the addition of an y-style splitter (1.6 mm, 10828; Ibidi) placed 11.5 cm from the inlet of the μ-Slide. To the y-style splitter, 20 cm of additional biocompatible silicone tubing (1.6 mm; 10828; Ibidi) was attached which was clamped off during biofilm growth using a hose clip (10821; Ibidi). For the experiment, the flow by the Ibidi pump system was stopped and the perfusion set clamped just after the additional y-style splitter. Then, the tubing was cut just under the original y-style splitters on both sides of the perfusion set, the additional tubing unclamped, and attached to a syringe pump (Pump 11 Elite, Harvard Apparatus, Holliston, Massachusetts, USA) so that injected fluid and vMB passed the biofilm only once (Fig. 2E). A solution of 200 μL IMDM containing 1.2 × 10^7 vMB (lipid conjugate batch EU) and 1% BSA was added into the in-line Luer injection port as described under 2.4.3. After 5 min of incubation, a shear stress of 1.5 dyn/cm^2 was applied for 60 s to remove unbound vMB from the biofilm. The transducer was operated in a 7° angle at 10% transmit power, medium beamwidth and 40 dB dynamic range and manipulated using a 3D acquisition motor (FUJIFILM VisualSonics) with a step size of 0.04 mm. Burst mode was used 1, 5 and 10 times to locally destroy vMB. B-mode and non-linear contrast mode were used to acquire images. Vevo LAB software was used to determine the mean contrast power and for rendering volume projections of 6.52 mm non-linear contrast scans.

2.7. Statistical analysis

All data were statistically analyzed using IBM SPSS Statistics 27 (IBM Corporation, Armonk, New York, USA), and a p-value of < 0.05 was used as the significance level. Data distribution was assessed using the Shapiro-Wilk test. The data on the microbubble size distribution, competitive microbubble binding assay, stability and microbubble binding under increasing shear stress was not normally distributed and was compared by performing a Mann-Whitney U test. To further analyze the competitive microbubble binding assay data, the Spearman's rank-order correlation was evaluated in MATLAB. The sonobactericide therapy data was not normally distributed and the robust test of equality of

means showed to be significant, so a Welch's *t*-test was performed instead. Normally distributed data of the non-specific vMB binding assay was compared using an unpaired *t*-test or one-way ANOVA with post-hoc Tukey HSD test for multiple groups.

3. Results

3.1. Conjugation of vancomycin to phospholipid and incorporation in the microbubble shell

The freeze-dried product obtained after dialysis was analyzed by mass spectrometry in order to assess the formation of the expected DSPE-PEG(3400)-vancomycin conjugate. Electrospray experiments were performed on the freeze-dried product containing both the lipid and the expected lipid conjugate. The multiplicity of PEG units in the lipid and the presence of the chlorine isotopes in vancomycin led to intricated spectra where the average molecular weight (MW) determination of the conjugate was not possible. According to MALDI-TOF experiments, the starting lipid was found to have a MW of ~4260 (Fig. 3A). The presence of the starting lipid and a second compound with an average MW of 5691, matching with the expected conjugate of ~5700, was confirmed for the freeze-dried product (Fig. 3B). Successful conjugation between the DSPE-PEG(3400)-NHS and vancomycin was further confirmed by TLC (Fig. S1).

The number weighted mean diameter of the vMB produced with the lipid conjugate (batch USA) or lipid conjugate (batch EU) did not show a significant difference between batches ($p = 0.737$). When comparing the number weighted diameter of vMB (median: 3.97, interquartile range: 0.52) to cMB diameter (median: 3.83, interquartile range: 0.58) (Fig. 4A), no significant difference was found ($p = 0.604$). The number weighted diameter of vMB does not indicate changes in microbubble size over the three-day period in which the experiments were performed. Fig. 4B shows similar polydisperse microbubble size distributions for vMB and cMB.

Incubation of vMB with a FITC-labeled anti-vancomycin antibody confirmed the presence of vancomycin as a ligand on the phospholipid coating using high-axial resolution 4Pi confocal microscopy. The patch-like FITC-signal within the three-dimensional reconstruction of the vMB, as seen in Fig. 5A, indicates that vancomycin is heterogeneously distributed over the vMB coating. The corresponding 4Pi confocal microscopy recording is shown in Video 1. The absence of any FITC-signal in the cMB (Fig. 5D) shows that there was no non-specific binding of the FITC-labeled anti-vancomycin antibody to the other phospholipid components. The corresponding 4Pi confocal microscopy recording is shown in Video 2. The destroyed freeze-dried vMB samples contained 3.23 and 2.69 μg/mL of vancomycin, corresponding to an average of 0.035 μg of vancomycin per mg of destroyed freeze-dried vMB. The lipid conjugate samples contained 87.46 and 60.43 μg/mL vancomycin, corresponding to an average of 41.41 μg vancomycin per mg of lipid conjugate. The average vancomycin loading efficiency was calculated to be 0.71%. The average number of vancomycin molecules per μm^2 of microbubble shell was calculated to be 5358 (5285 and 5431 molecules).

3.2. Binding of targeted microbubbles to bacteria in biofilms

The ability of vMB and cMB to bind to statically grown biofilms was assessed with a competitive microbubble binding assay (Fig. 6). Significantly more vMB were found at the bacterial biofilms compared to cMB, regardless of the concentration of free vancomycin present. For vMB, increasing the concentration of free vancomycin up to 20 μg/mL prior to the incubation with vMB did not result in a significant decrease in the amount of bound vMB. Only the preincubation of biofilms with a free vancomycin concentration greatly exceeding the maximal clinical dose of 20 μg/mL, namely 100 and 1,000 μg/mL, reduced the number of bound vMB (respectively, $p = 0.02$ and $p < 0.001$). No significant difference ($p = 0.74$) was found between the binding of vMB produced with either the USA or EU lipid conjugate batch. There was no significant difference ($p = 0.065$) between the number of cMB after preincubating without or with 1,000 μg/mL of vancomycin. Furthermore, using the same data as in Fig. 6 the number of vMB and cMB was found to be unaffected by the location within the μ-Slides (Fig. S2). At most a moderate negative correlation (i.e. number of microbubbles moderately decreases as the distance from the inlet increases) was observed for two conditions, both with vMB, with a free vancomycin concentration of 10 μg/mL ($r = -0.53$, $p < 0.001$) and 1,000 μg/mL ($r = -0.54$, $p < 0.001$). All

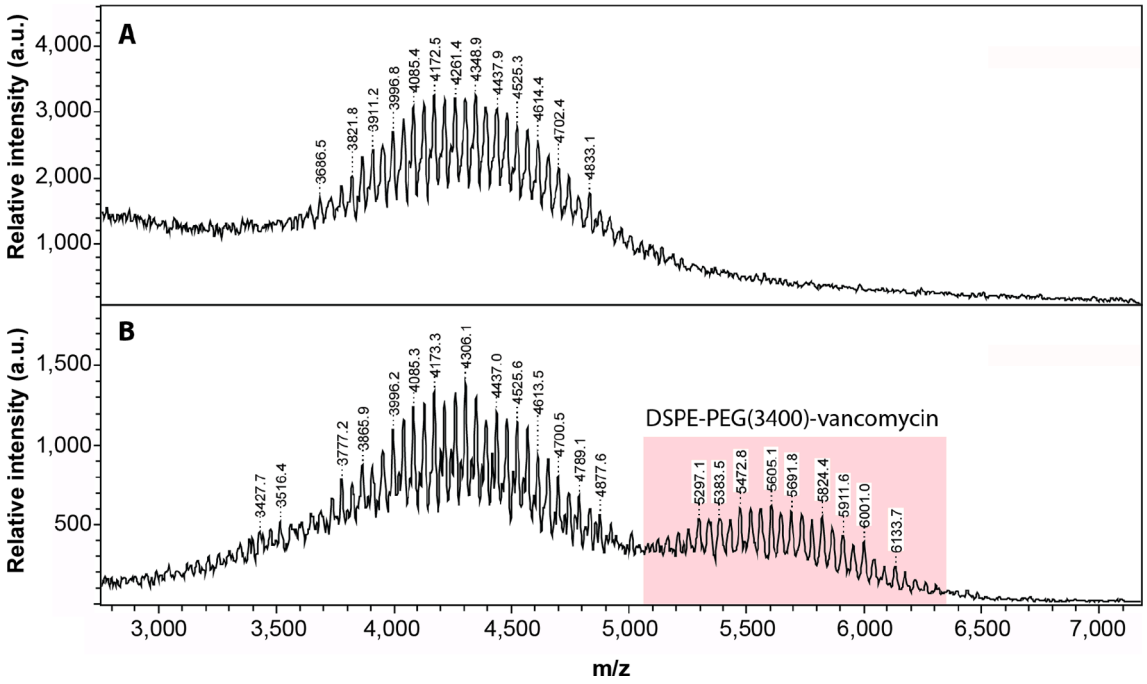

Fig. 3. Matrix-assisted laser desorption/ionization - time-of-flight mass spectra of (A) DSPE-PEG(3400) and (B) the freeze-dried product after dialysis with the red shaded region confirming the vancomycin coupled to the polyethylene-glycol (PEG) lipid.

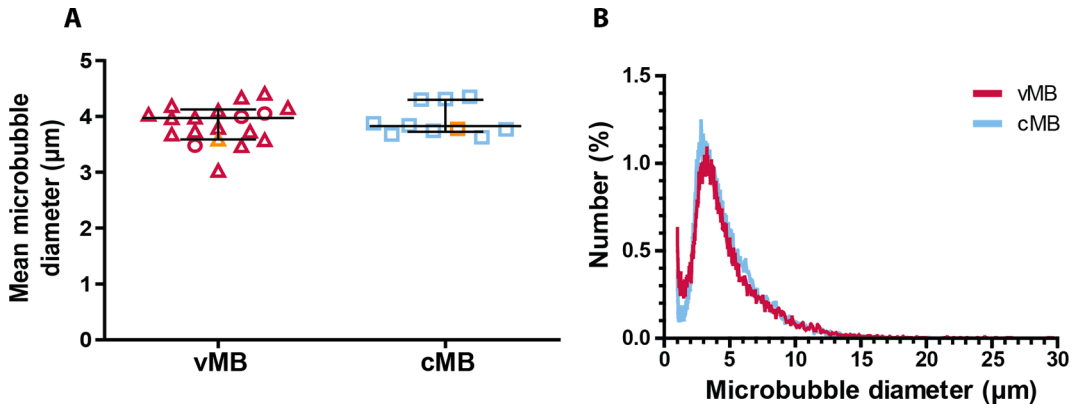

Fig. 4. Microbubble number-weighted mean diameter and size distribution. (A) The mean diameter of vancomycin-decorated microbubbles (vMB, red, n = 19 batches) and control microbubbles (cMB, blue, n = 10 batches) used in all experiments. The vMB were produced with either lipid conjugate batch USA (red circles) or lipid conjugate batch EU (red triangles). The median and interquartile range are overlaid. Orange-colored symbols indicate the MB batches corresponding to those represented in B. (B) Representative size distribution of vMB and cMB batches.

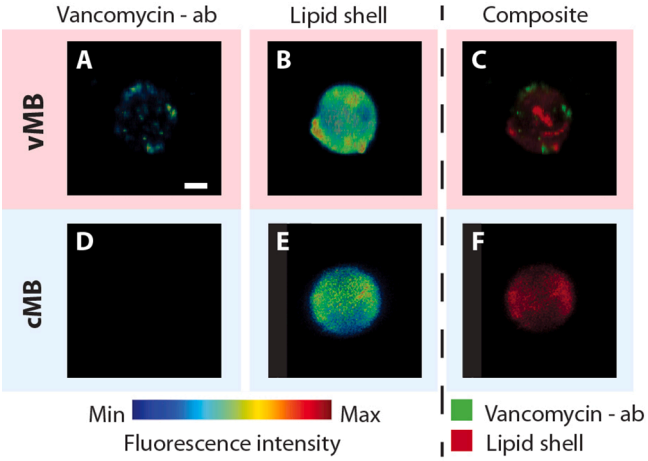

Fig. 5. Representative 3D reconstructions of high-axial resolution 4Pi confocal microscopy y-stacks of (A-C) a vancomycin-decorated microbubble (vMB, diameter = 4.2 µm) and (D-F) a control microbubble (cMB, diameter = 4.3 µm). (A, D) Fluorescence intensity images of the FITC-labeled anti-vancomycin antibody (vancomycin-ab) and (B, E) the phospholipid shells with the lipid dye DiD for vMB and DiI for cMB. (C, F) The composite image of the fluorescence emitted by the FITC-labeled anti-vancomycin antibody (green) and lipid dye (red). Scale bar is 1 µm and applies to all images.

other conditions had coefficient values <0.4 (r values ranging from −0.33 to 0.13), which indicate little to no relationship between the two variables. The stability of the vMB did not decrease during the three-day period the microbubbles were used for experiments (Fig. S3). On day 3 there was even a slight but significant increase in the number of bound vMB ($p < 0.05$).

cMB showed negligible non-specific binding to the µ-Slides without biofilm. Fig. 7 shows that the percentage of vMB bound to the µ-Slide without biofilm was approximately two-thirds of the percentage of vMB bound to biofilms. When 0.1% BSA was added, the percentage of vMB bound to the µ-Slide without biofilm significantly ($p < 0.05$) dropped, while no significant changes ($p = 0.51$) were observed for the vMB bound to biofilms. When the BSA concentration was increased to 1%, the same trend was visible; a significant decrease in the percentage of vMB bound to the µ-Slide without biofilm ($p < 0.05$) and no significant differences ($p = 0.13$) in the percentage of vMB bound to the biofilm. Similar results were obtained when BSA was substituted for casein (Fig. S4).

To determine the number of microbubbles that remained bound under flow, the vMB and cMB were distinguished by the different lipid dyes incorporated into their coating as shown in Fig. 8B, E and C, F, respectively. The average number of vMB present before flow was 51 ± 37 and for cMB 61 ± 44 (mean ± SD; n = 8) per field-of-view, and the ratio of vMB/cMB was 0.87 ± 0.16. Time-lapse imaging while flow shear stress increased from 1.5 to 12 dyn/cm^2 was performed to distinguish bound from unbound microbubbles and revealed that vMB had a significantly higher binding percentage in comparison to cMB at all shear stress values, except from 7 to 9 dyn/cm^2 (Fig. 8G). The biofilm remained attached to the microchannel throughout the duration of flow binding experiments (Fig. 8A,D).

3.3. Sonobactericide with vancomycin-decorated microbubbles

Biofilms grown under flow had a field-of-view coverage of 89.7 ± 10.7% (mean ± SD) (n = 22 fields-of-view in 11 different µ-Slides). A typical example of a biofilm treated with sonobactericide using vMB is shown in Fig. 9, where five vMB (diameter ranging from 2.0 to 4.5 µm) remained attached to the biofilm under flow (5 dyn/cm^2) before

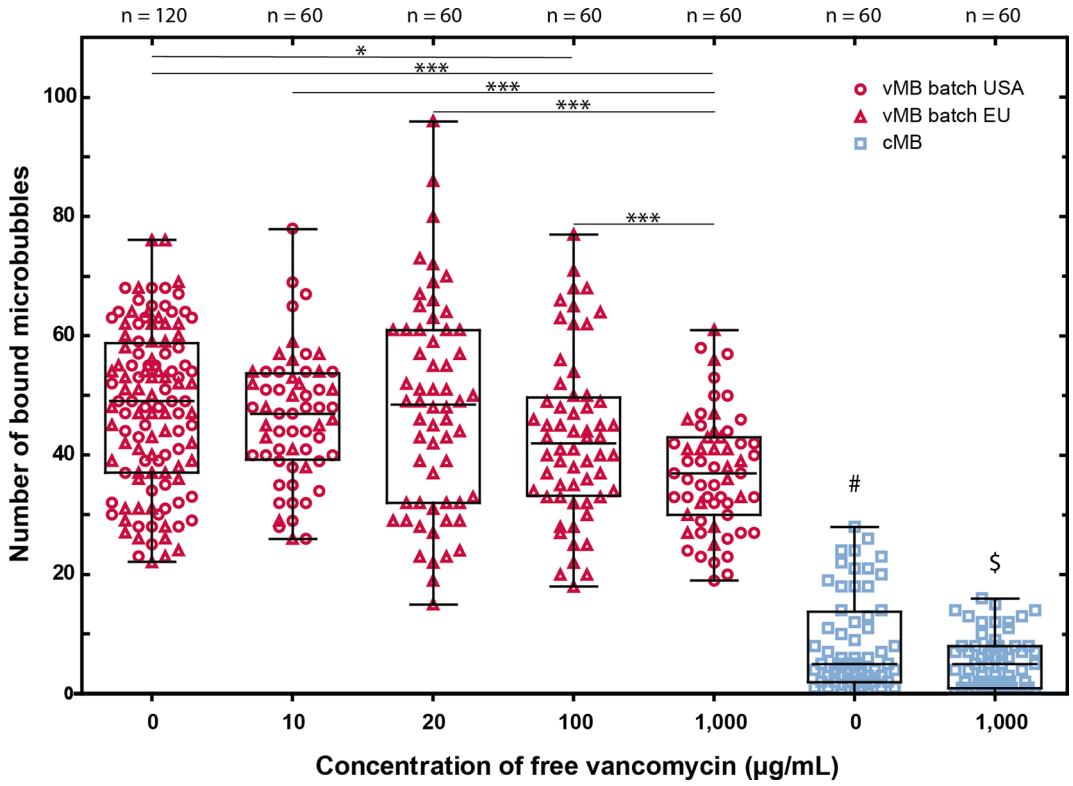

Fig. 6. The number of bound vancomycin-decorated (vMB, red symbols) and control (cMB, blue squares) for varying concentrations of free vancomycin with statically grown biofilms. The vMB were produced with either lipid conjugate batch USA (red circles) or batch EU (red triangles). Each symbol represents the number of microbubbles counted in one field-of-view. The overlaid boxplots show the median, interquartile range, and the minimum to maximum values. Statistical significance for vMB is indicated with * ($p < 0.05$) or *** ($p < 0.001$) when comparing different free vancomycin concentrations, # ($p < 0.001$) when comparing cMB without free vancomycin to all vMB conditions, and $ ($p < 0.001$) when comparing cMB with 1000 µg/mL free vancomycin to all vMB conditions.

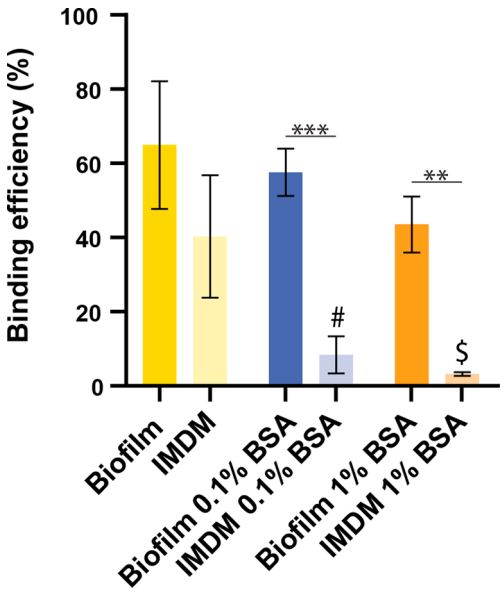

Fig. 7. Non-specific binding of vancomycin-decorated microbubbles. Ibidi µ-Slides with and without statically grown biofilms in IMDM were incubated with either 0 %, 0.1 % or 1% bovine serum albumin (BSA) to bind to non-specific binding sites. Each bar represents the mean binding efficiency percentage with standard deviation overlaid of n = 3. Statistical significance is indicated with ** ($p < 0.01$), *** ($p < 0.001$), # ($p < 0.05$) between IMDM 0.1% BSA and all other conditions except for IMDM 1% BSA, and $ ($p < 0.05$) between IMDM 1% BSA and all other conditions except for IMDM 0.1% BSA.

ultrasound treatment (Fig. 9A). Upon ultrasound insonification using 5,000 cycles, all vMB displaced from the field-of-view resulting in a 24.0% reduction in biofilm area localized along the microbubble displacement trajectories (Fig. 9B). The corresponding confocal microscopy recording is shown in Video 3. Overall, biofilms (n = 7) treated with vMB and a single ultrasound burst of 5,000 cycles resulted in a median reduction of 19.6% (interquartile range 11.5%; Fig. 9C). When vMB were exposed to 10,000 cycles, a more consistent biofilm reduction amount was observed, with the highest being 27.6% and a median of 20.8% (interquartile range 6.3%; n = 4; Fig. 9C), albeit not significantly different from 5,000 cycles. No noticeable increase in PI positive cells was observed following all treatments. Both ultrasound settings in combination with vMB resulted in significantly higher biofilm area reduction than any of the control treatments (imaging under flow only, vMB only, and ultrasound only). Similar low percentages (<6.3%) of biofilm area reduction were obtained for all control treatments partly due to focus drift during the confocal microscopy recordings and biofilm erosion.

To visualize the effect of the sonobactericide treatment on a microsecond time scale, Brandaris 128 ultra-high-speed camera recording was combined with time-lapse confocal microscopy. Fig. 10A shows an example of a selected confocal microscopy frame of a biofilm with two vMB (diameter 6.3 µm and 4.3 µm) attached under flow before ultrasound insonification. During continuous flow, the vMB were simultaneously insonified (5,000 cycles) and the largest vMB in the middle of the field-of-view recorded at an ultra-high-speed for the first 14 cycles, where selected frames of this recording are shown in Fig. 10B. Throughout the Brandaris 128 recording (Fig. 10E), the vMB remained bound to the bacterial biofilm and the microbubble oscillation amplitude was determined in each frame, resulting in a diameter range from 4.7 µm to 7.8 µm during ultrasound exposure. The corresponding

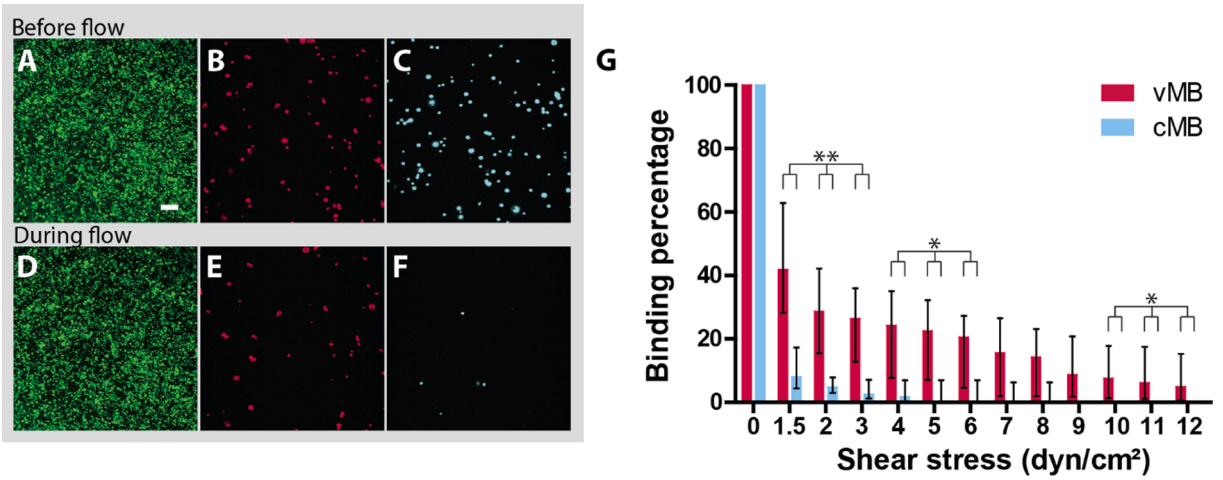

Fig. 8. Percentage of microbubbles that remained bound upon increasing shear stress with flow grown biofilms. Confocal microscopy images of (A-C) the initial state before flow and (D-F) after 60 s of 1.5 dyn/cm^2 shear stress flow. Both sets of images are the same biofilm with (A, D) bacteria stained with SYTO 9 (green), (B, E) vancomycin-decorated microbubbles (vMB) stained with DiD (red), and (C, F) control microbubbles (cMB) stained with DiI (blue). Scale bar is 20 μm and applies to all confocal images. (G) Bars represent median percentage with interquartile range of microbubbles in the field-of-view remaining bound to the bacterial biofilm during increasing shear stress (n = 8). Statistical significance between bound vMB percentage and bound cMB percentage is indicated with * ($p < 0.05$) or ** ($p < 0.01$).

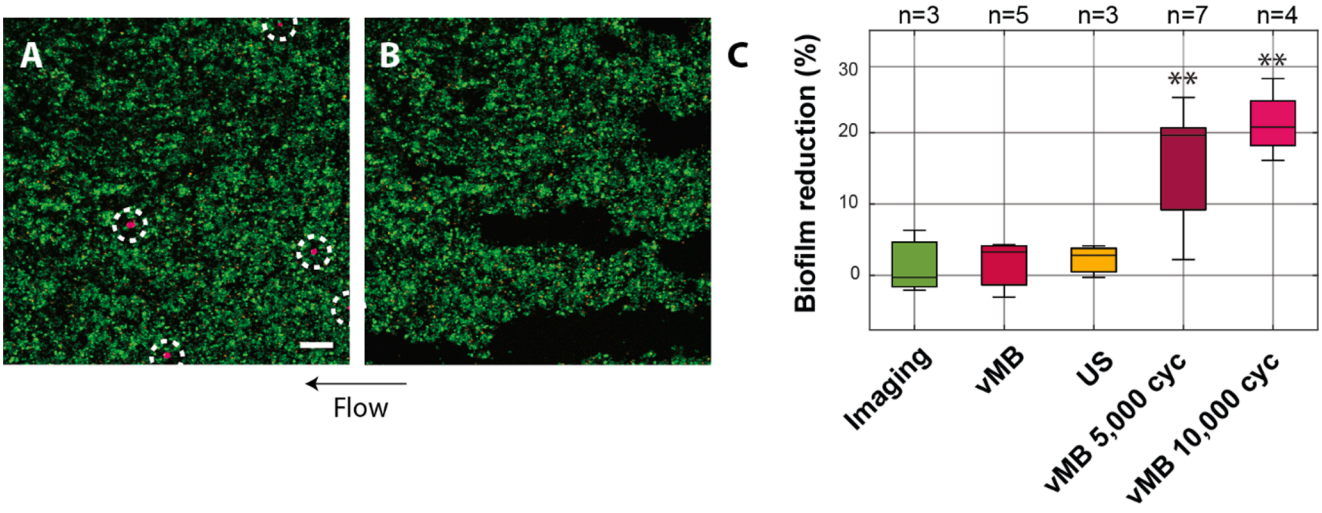

Fig. 9. Biofilms treated under flow at 5 dyn/cm^2 with vancomycin-decorated microbubbles (vMB) and ultrasound. Confocal microscopy images of (A) before and (B) after sonobactericide treatment (2 MHz, 250 kPa, 5,000 cycles. Live bacteria were stained with SYTO 9 (green), dead bacteria with propidium iodide (orange), and vMB with DiD (red; indicated by white dashed circles). Scale bar is 20 μm and applies to all confocal images. (C) Percentage of biofilm reduction upon treatment. Boxplots show the median, interquartile range, and the minimum to maximum values. The ultrasound (US) setting of 2 MHz, 250 kPa, 10,000 cycles was used for US alone. Statistical significances between vMB in combination with US and the control treatment groups are indicated with ** ($p < 0.01$); cyc = cycles.

Brandaris 128 recording is shown in Video 4. After ultrasound insonification, the effect of the oscillating vMB on the biofilm was clearly visible (Fig. 10C), where approximately 606.1 μm^2 was removed, corresponding to a 3.7% total reduction in the field-of-view. This reduction is within the range observed for this insonification as shown in Fig. 9C, even though the magnification was higher.

3.4. Ultrasound molecular imaging

B-mode images of μ-Slides without biofilm showed minimal ultrasonic signal compared to μ-Slides containing biofilms (Fig. S5). Nonlinear contrast mode imaging showed only minimal signal for μ-Slides without biofilm (Fig. 11A). When a biofilm grown under flow was imaged in non-linear contrast mode, thicker parts of the biofilm could be detected in the microchannel before the introduction of vMB (Fig. 11B). After incubation with vMB (Fig. 11C), the contrast-to-tissue ratio increased dramatically by 20.2 dB. The ultrasound molecular signal, with an 18.1 dB contrast-to-tissue ratio, only slightly decreased after washing away unbound vMB (Fig. 11D). To confirm that the non-linear signal was generated by the vMB, bursts were applied on three different places resulting in three individual lines across the 3D rendered image (Fig. 11E) where the vMB were destroyed.

4. Discussion

In this study, a novel targeted microbubble was successfully developed based on the NHS ester chemical reaction that resulted in the coupling of the antibiotic vancomycin to the microbubble coating. Furthermore, using bacteria-associated biofilms, ultrasound, and flow, the theranostic proof-of-principle was demonstrated for the first time using a vMB and ultra-high-speed recording of the microbubble oscillation behavior. Targeting microbubbles directly to biofilms has the

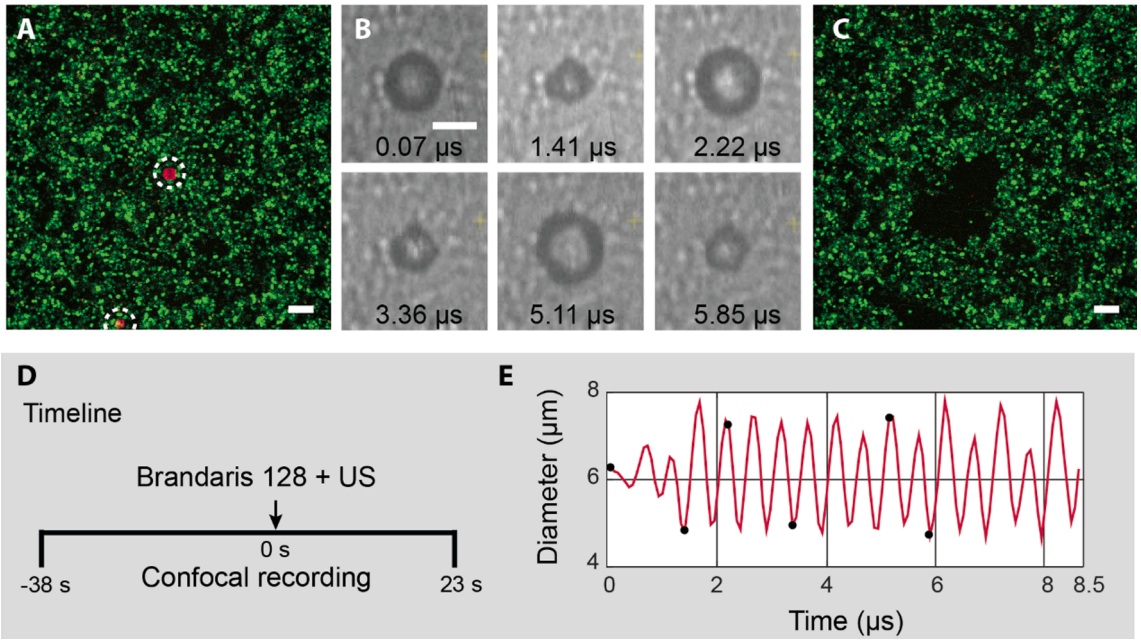

Fig. 10. Theranostic potential of vancomycin-decorated microbubble (vMB) upon ultrasound under flow (5 dyn/cm^2). (A) Initial state confocal microscopy image of vMB (red, DiD stained; indicated by white dashed circles) bound to bacteria (green, SYTO 9 stained) ~ 1 s before ultrasound exposure. Dead bacteria were stained with propidium iodide (orange). Scale bar is 10 μm and also applies to C. (B) Selected frames of Brandaris 128 ultra-high-speed camera recording showing the vMB in the center of A oscillating in response to a single burst of ultrasound (US; 2 MHz, 250 kPa, 5,000 cycles). Scale bar is 5 μm. (C) Corresponding confocal image ~ 3 s after ultrasound exposure showing biofilm disruption. (D) Imaging timeline during recordings. (E) Microbubble diameter as a function of time visualizing the oscillation behavior of the microbubble during ultrasound insonification. The black dots correspond to the selected images in B.

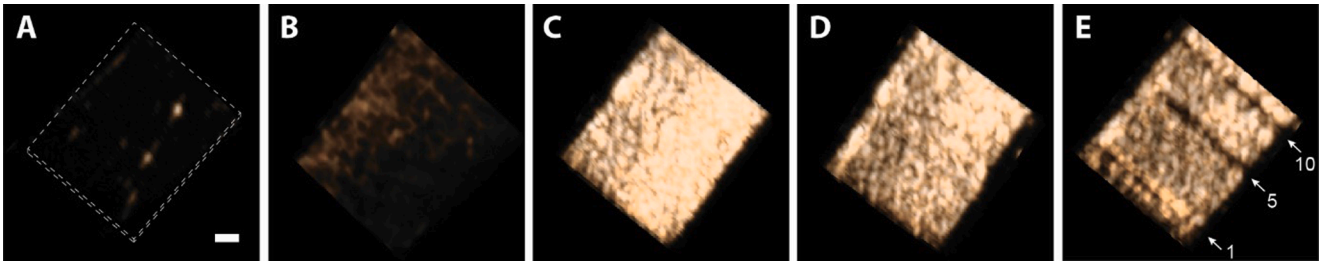

Fig. 11. Ultrasound molecular imaging of biofilm. 3D rendered non-linear contrast image of the microchannel of a μ-Slide (A) without biofilm (microchannel delineated by the white dashed rectangle), (B) with biofilm before addition of vancomycin-decorated microbubbles (vMB), (C) with biofilm after incubation with vMB, (D) with biofilm after incubation and washing away unbound vMB, and (E) after applying 1, 5 or 10 flash bursts (white arrows followed by 1, 5 and 10). Scale bar is 1 mm and applies to all images.

potential to further enhance therapy and provide a diagnostic component at the same time, both of which are desperately needed.

4.1. Successful conjugation of vancomycin to phospholipid and incorporation in the microbubble shell

The coupling of vancomycin to the microbubble phospholipid component DSPE-PEG(3400) was done via the NHS ester functional group of the lipid and primary amine of the vancomycin, a method also used by others for coupling vancomycin to a fluorescent dye (van Oosten et al., 2013). MALDI-TOF mass spectrometry confirmed successful conjugation, where the starting material only shows a peak at around ~4260 Da and all conjugated samples had a second peak at ~5700 Da indicating the conjugate (Fig. 3). However, due to the chloride isotopes of vancomycin and multiplicity of the lipid's PEG-tail, it was not possible to determine the exact ratio between starting materials and final conjugate. The 4Pi microscopy data shows that the vancomycin was heterogeneously distributed over the microbubble coating after production (Fig. 5). This heterogeneous ligand distribution might play a role in binding given that not every part of the microbubble coating can bind to bacteria. Although heterogeneous ligand distributions have previously been reported for DSPC-based microbubbles (Kooiman et al., 2014; Borden et al., 2006), a more homogeneous distribution could increase the probability of the vMB to bind to the bacteria. Lipid handling prior to microbubble production (Langeveld et al., 2020) or different heating–cooling protocols after microbubble production (Borden et al., 2006) have been shown to alter ligand distribution to become homogeneous in DSPC-based microbubbles, but these require organic solvents or high temperatures which may compromise vancomycin functionality. One of the possibilities to improve the binding profile of the vMB is to expand the purification process of the lipid conjugate after dialysis.

The antimicrobial property of vancomycin coupled to a microbubble coating should still be present since the binding site used to inhibit cell wall synthesis remains intact after conjugation. The overall therapeutic effect of the conjugated vancomycin alone is then only limited by the amount that is coupled and how many bacteria can bind to each microbubble. By determining the vancomycin concentration on the vMB, the amount of vancomycin in a clinical dose of 1×10^9 vMB (Lumason., 2016) was calculated to be 0.78 μg. This is extremely low when considering that the clinical target serum concentration of

vancomycin is 15–20 μg/mL (Pritchard et al., 2010; Tongsai and Koomanachai, 2016). On the other hand, the calculated average number of 5358 vancomycin molecules per μm^2 of microbubble shell is in the similar range as the previously reported ~2500 antibody molecules for P-selectin targeted lipid coated microbubbles (Takalkar et al., 2004). Although microbubble coating coverage is crucial when considering it may increase chances of microbubble binding *in vivo,* the therapeutic enhancement effects that vMB can provide lies more on the ultrasound-mediated microbubble behavior. This includes the potential to decrease the current dosage of vancomycin necessary for patients, which could lower the incidence of antibiotic-induced nephrotoxicity.

4.2. Successful binding of targeted microbubbles to bacteria in biofilms

Almost all sonobactericide studies use static biofilm cultivation (Lattwein et al., 2020). For some research questions and target diseases, static biofilms are adequate. However, to also include flow-related biofilm-mediated diseases, the addition of multiple flow shear stresses to the biofilm model was pivotal. This addition, in combination with the human plasma coating, resulted in differently grown biofilms which often had a more three-dimensional structure to it than statically grown biofilms. Our vMB successfully bound to bacteria and remained bound through increasing shear stresses of up to 12 dyn/cm^2 (Fig. 8). Although the maximal shear stress used in this *in vitro* model is on the lower spectrum in healthy human arteries (10–70 dyn/cm^2), it is above the shear stress found in healthy veins (1–6 dyn/cm^2) (Malek et al., 1999). Binding of targeted microbubbles under high shear stress conditions can be challenging. To bypass this problem, one could make use of primary acoustic radiation forces. *Dayton et al.* (Dayton et al., 1999) and *Rychak et al.* (Rychak et al., 2005; Rychak et al., 2007) showed that this phenomenon increases microbubble binding in flow conditions by displacing microbubbles towards the desired binding area *in vitro* and *in vivo*; while also significantly reducing the flow speed of these microbubbles. Theoretically, this approach can increase the number of targeted microbubbles binding to biofilms. Another consideration is that the circulatory system experiences pulsatile flow with each heartbeat. The lull between each cyclical increase and decrease in flow and the forwards and backwards motion of fluid, both due to pulsatile flow, could provide enough time for vMB to bind compared to a continuous flow state. It therefore is of interest for future studies to investigate binding under flow using ultrasound and pulsatile flow, potentially providing an even better binding profile of vMB.

A factor that could affect vMB binding success is that patients are started on antibiotic therapy the moment infection is suspected, which means that the available binding sites could already be occupied before vMB are administered. Therefore, competition was assessed using free vancomycin concentrations ranging from 0 to 1000 μg/mL (Fig. 6), and no significant differences were observed between 0 and 20 μg/mL, which is the clinical dose. This lends support that vMB can still be used as a theranostic whether or not the patient is already on high-concentration vancomycin therapy. Another factor which can also affect vMB efficiency is plasma protein binding. For free vancomycin, this has been reported as approximately 26% (Stove et al., 2015), which could also be the case for vMB. It is also possible that if vancomycin is administered to the patient before vMB are infused, it could minimize the off-target binding to plasma proteins and other potential non-desired attachment. Nonetheless, experiments need to be performed in order to make this determination.

Variability was seen in the number of bound vMB (Fig. 6), which partly could be explained by the heterogenous nature of biofilms, such as differences in the amount and accessibility of the D-Ala-D-Ala moiety of the bacteria in the biofilm. This relation between binding of targeted microbubbles and the density of the biomarker is clearly demonstrated by *Takalkar et al.* (Takalkar et al., 2004) in their *in vitro* study using anti P-selectin antibody microbubbles and P-selectin as biomarker. Likely, this variability can also partly be explained by the fluctuation in the number of microbubbles entering the microchannel of the Ibidi μ-Slide. Regardless, the number of bound vMB for each condition was all significantly higher than the cMB groups. cMB did exhibit some non-specific binding to the biofilm (Fig. 6), however this was minor and known to also occur with non-targeted microbubbles for mammalian cells (Bettinger et al., 2012; Wang et al., 2016; Daeichin, 2016). Under flow conditions the cMB adherence to biofilms, for example at 1.5 dyn/cm^2 (Fig. 8G), could in fact be due to the natural rough, irregular surface of biofilms preventing microbubbles from moving away and requiring a certain level of flow to overcome this. cMB binding results were significantly different than vMB, both in number of microbubbles bound statically and in their ability to withstand flow, except for 7 to 9 dyn/cm^2 which could also be explained by microbubbles getting stuck in the biofilm's irregular surface (e.g., protuberances) without binding. Higher flow shear stresses remove the residual unbound control microbubbles from the irregular surface while vMB remained bound. To minimize the effect heterogenous biofilms could have on the binding percentage, both vMB and cMB were tested together in the flow experiments at a 1:1 ratio. However, the ratio in the fields-of-view was found to be 0.87:1, and therefore the percentage in the microbubble binding under increasing shear stress represents a smaller number of vMB compared to cMB. It is possible that vMB could have bound to bacteria potentially growing within the tubing set or inlet, and/or planktonic bacteria in the media before reaching the field-of-view within the μ-Slides resulting in the lower amount of vMB in comparison to cMB.

The non-specific binding of vMB found in μ-Slides only containing IMDM, i.e. without biofilm, (Fig. 7) was likely due to electrostatic non-specific binding to the microchannel of the μ-Slide. When 0.1% or 1% BSA was added to the vMB solution, this non-specific binding was significantly decreased while maintaining the specific binding to the bacterial biofilm. No similar non-specific binding is expected *in vivo*, since human serum albumin is abundantly present in the bloodstream, i.e. up to 5.5% (Burtis and Bruns, 2014).

4.3. Theranostic proof-of-principle of vancomycin-decorated microbubbles

This study provides diagnostic and therapeutic proof-of-principle by showing vMB response upon ultrasound insonification. The ability of bound vMB to biofilms to generate an echogenic signal in non-linear contrast mode (Fig. 11) shows vMB could be used to detect early biofilm development via ultrasound molecular imaging, for which up till now no single suitable detection method is available. Using the Brandaris 128 ultra-high-speed camera, a vMB under flow was shown to exhibit oscillations upon insonification while staying bound to the biofilm (Fig. 10). Concerning therapeutic potential, vMB bound to bacteria were able to significantly disrupt biofilms when exposed to ultrasound (Fig. 8). This conforms to other reports from sonobactericide papers where non-targeted microbubbles combined with ultrasound can have a therapeutic effect on *in vitro* and *in vivo* biofilms (Lattwein et al., 2020). However, this study revealed some different biofilm reduction effects which might be contributed to targeted microbubbles and flow. Specifically, the streak pattern and large amount of reduction caused by individual microbubbles and one burst of ultrasound versus the craters and holes that others report by concentrated non-targeted microbubbles and different insonification schemes. Biofilm reduction was most likely caused by the microbubble oscillatory mechanical effects (Fig. 10), such as microstreaming in combination with flow. Regardless of the mechanism, damaged biofilms become more sensitive to antibiotics (Wille and Coenye, 2020), which could translate to shorter duration and lower dosage of antibiotics needed to achieve biofilm eradication.

Direct bacterial killing could also occur and in a manner of two avenues. Firstly, the vancomycin on vMB bound to bacteria still has the ability to kill via the same mechanisms as free vancomycin. Secondly, ultrasound-induced microbubble behavior could enhance membrane permeabilization ultimately leading to cell death, as observed in

mammalian cells (van Rooij et al., 2016). The PI fluorescence stain is commonly used as a marker of cell death, as used in this study to assess the initial state of bacteria within biofilms, but also as a permeabilization marker since it is cell impermeable to intact membranes. However, direct PI uptake after sonobactericide treatment was not observed in this study. This could be due to bacterial cells requiring more time to die following membrane damage and dispersed cells not being trackable outside of the field-of-view, since other studies report higher PI positive cell numbers but only seen by optical imaging minutes to days after insonification (Lattwein et al., 2020). The therapeutic impact of one bound vMB is probably multifaceted, with direct and indirect consequences on both the bacteria and biofilm structure.

While this new approach shows promise to improve biofilm infection patient outcomes, it needs to be certain that vMB do not contribute to bacterial dispersal and or the release of biofilm fragments into the circulation. Bacteria that are dispersed or dislodged from biofilms due to vMB should be characterized to understand and be able to address the potential risks to be viable as a therapeutic (Wille and Coenye, 2020; França et al., 2016). For vMB as a diagnostic, less risk is envisioned since the ultrasound settings used would remain within a few cycles and on the lower acoustic pressure spectrum not intended to induce major bioeffects. It is expected that the vMB itself will not contribute to adverse effects. The main compound, DSPC, is also the main component of SonoVue microbubbles which are already safely used in the clinic for several decades (Lv, 2021). PEG-40 stearate is widely used as an emulsifier in microbubble formulations (Owen et al., 2019; Xing et al., 2010; Dixon et al., 2013). The gas used to produce the vMB, C_4F_{10}, is a component of Sonazoid, another clinically approved microbubble (Chou et al., 2019). Although in this study DSPE-PEG(3400) was used to couple vancomycin, the comparable DSPE-PEG(2000) is a component of the BR55 microbubble, which has shown safety in clinical trials (Willmann et al., 2017). Vancomycin as an antibiotic is used in the clinic with minimal side-effects (Rubinstein and Keynan, 2014).

5. Conclusion

In this study, to the best of our knowledge for the first time, vMB were produced and characterized which showed successful incorporation of the antibiotic vancomycin to the microbubble's lipid shell. Confocal microscopy revealed that vMB were able to bind to *S. aureus* biofilms and remained attached under increasing physiological flow conditions. Significant biofilm reduction was seen upon ultrasound-activation of vMB. vMB oscillation under flow was visualized on a microsecond time-scale using the Brandaris 128 ultra-high-speed camera. Bound vMB to the biofilm evidently enhanced the ultrasound signal during ultrasound molecular imaging. The ability of vMB to bind to biofilms combined with the mechanical effects induced upon ultrasound insonification have promising potential to both enhance treatment through sonobactericide and provide early diagnosis by ultrasound molecular imaging of biofilm-mediated diseases.

CRediT authorship contribution statement

Joop J.P. Kouijzer: Conceptualization, Methodology, Validation, Formal analysis, Investigation, Data curation, Writing – original draft, Writing – review & editing, Visualization, Project administration. **Kirby R. Lattwein:** Conceptualization, Methodology, Investigation, Writing – original draft, Writing – review & editing. **Inés Beekers:** Software, Validation, Formal analysis, Investigation, Writing – review & editing. **Simone A.G. Langeveld:** Methodology, Validation, Investigation, Writing – review & editing, Visualization. **Mariël Leon-Grooters:** Investigation, Writing – review & editing. **Jean-Marc Strub:** Methodology, Validation, Investigation, Writing – review & editing. **Estefania Oliva:** Methodology, Validation, Investigation, Writing – review & editing. **Gaëtan L.A. Mislin:** Methodology, Validation, Investigation, Writing – review & editing, Visualization. **Nico Jong:** Conceptualization, Writing – review & editing, Supervision. **Antonius F. W. Steen:** Resources, Supervision, Funding acquisition. **Alexander L. Klibanov:** Methodology, Writing – review & editing. **Willem J.B. Wamel:** Conceptualization, Resources, Supervision. **Klazina Kooiman:** Conceptualization, Methodology, Resources, Writing – review & editing, Supervision, Funding acquisition.

Declaration of Competing Interest

The authors declare that they have no known competing financial interests or personal relationships that could have appeared to influence the work reported in this paper.

Acknowledgements

This project has received funding from the European Research Council (ERC) under the European Union's Horizon 2020 research and innovation program [grant agreement 805308)]. Gaëtan Mislin acknowledges the Interdisciplinary Thematic Institute (ITI) InnoVec (Innovative Vectorization of Biomolecules, IdEx, ANR-10-IDEX-0002) and SFRI (ANR-20-SFRI-0012). The authors would like to thank Robert Beurskens, Frits Mastik and Reza Pakdaman Zangabad from the Department of Biomedical Engineering, Michiel Manten from the Department of Experimental Medical Instrumentation, Andi R. Sultan from the Department of Medical Microbiology and Infectious Diseases and Ruud Huisman from the Department of Hospital Pharmacy, all from the Erasmus University Medical Center Rotterdam, for their skillful technical assistance. The authors thank the Optical Imaging Centre of Erasmus MC for the use of their facilities and Gert van Cappellen and Alex Nigg for their help. The authors also thank the members of the Therapeutic Ultrasound Contrast Agent group (Biomedical Engineering Dept.) and the *S. aureus* working group (Medical Microbiology and Infectious Diseases Dept.) from Erasmus University Medical Center Rotterdam for their useful discussions.

Appendix A. Supplementary material

Supplementary data to this article can be found online at https://doi.org/10.1016/j.ijpharm.2021.121154.

References

Anastasiadis, P., et al., 2014. Detection and quantification of bacterial biofilms combining high-frequency acoustic microscopy and targeted lipid microparticles. J. Nanobiotechnology 12 (1), 24. https://doi.org/10.1186/1477-3155-12-24.

Bannay, A., et al., 2011. The impact of valve surgery on short- and long-term mortality in left-sided infective endocarditis: do differences in methodological approaches explain previous conflicting results? Eur. Heart J. 32 (16), 2003–2015. https://doi.org/10.1093/eurheartj/ehp008.

Beekers, I., et al., 2019. Combined Confocal Microscope and Brandaris 128 Ultra-High-Speed Camera. Ultrasound Med. Biol. 45 (9), 2575–2582. https://doi.org/10.1016/j.ultrasmedbio.2019.06.004.

Bettinger, T., et al., 2012. Ultrasound molecular imaging contrast agent binding to both E- and P-selectin in different species. Invest. Radiol. 47 (9), 516–523. https://doi.org/10.1097/RLI.0b013e31825cc605.

Bin Abdulhak, A.A., et al., 2014. Global and regional burden of infective endocarditis, 1990–2010: a systematic review of the literature. Glob. Heart 9 (1), 131. https://doi.org/10.1016/j.gheart.2014.01.002.

Borden, M.A., et al., 2006. Lateral phase separation in lipid-coated microbubbles. Langmuir 22 (9), 4291–4297. https://doi.org/10.1021/la052841v.

Broker, B.M., Holtfreter, S., Bekeredjian-Ding, I., 2014. Immune control of Staphylococcus aureus - regulation and counter-regulation of the adaptive immune response. Int. J. Med. Microbiol. 304 (2), 204–214. https://doi.org/10.1016/j.ijmm.2013.11.008.

Burtis, C.A., Bruns, D.E., 2014. Tietz fundamentals of clinical chemistry and molecular diagnostics-e-book. 2014: Elsevier Health Sciences.

Cassini, A., et al., 2019. Attributable deaths and disability-adjusted life-years caused by infections with antibiotic-resistant bacteria in the EU and the European Economic Area in 2015: a population-level modelling analysis. Lancet Infect Dis. 19 (1), 56–66. https://doi.org/10.1016/S1473-3099(18)30605-4.

Chen, X., et al., 2013. Ultra-fast bright field and fluorescence imaging of the dynamics of micrometer-sized objects. Rev. Sci. Instrum. 84 (6), 063701 https://doi.org/10.1063/1.4809168.

Chirouze, C., et al., 2004. Prognostic factors in 61 cases of Staphylococcus aureus prosthetic valve infective endocarditis from the international collaboration on endocarditis merged database. Clin Infect Dis 38 (9), 1323–1327. https://doi.org/10.1086/383035.
Chou, Y.-H., et al., 2019. Safety of perfluorobutane (sonazoid) in characterizing focal liver lesions. J Med Ultrasound 27 (2), 81. https://doi.org/10.4103/JMU.JMU_44_19.
Daeichin, V., et al., 2016. Quantification of endothelial alphavbeta3 expression with high-frequency ultrasound and targeted microbubbles. In vitro and in vivo studies. Ultrasound. Med. Biol. 42 (9), 2283–2293. https://doi.org/10.1016/j.ultrasmedbio.2016.05.005.
Daeichin, V., et al., 2017. Microbubble composition and preparation for high-frequency contrast-enhanced ultrasound imaging. In vitro and in vivo evaluation. IEEE Trans. Ultrason. Ferroelectr. Freq. Control 64 (3), 555–567. https://doi.org/10.1109/TUFFC.5810.1109/TUFFC.2016.2640342.
Dauty, E., et al., 2002. Intracellular delivery of nanometric DNA particles via the folate receptor. Bioconjug Chem. 13 (4), 831–839. https://doi.org/10.1021/bc0255182.
Dayton, P., et al., 1999. Acoustic radiation force in vivo: a mechanism to assist targeting of microbubbles. Ultrasound Med. Biol. 25 (8), 1195–1201. https://doi.org/10.1016/S0301-5629(99)00062-9.
DeSimone, D.C., Sohail, M.R., 2016. Management of bacteremia in patients living with cardiovascular implantable electronic devices. Heart Rhythm 13 (11), 2247–2252. https://doi.org/10.1016/j.hrthm.2016.08.029.
Dimcevski, G., et al., 2016. A human clinical trial using ultrasound and microbubbles to enhance gemcitabine treatment of inoperable pancreatic cancer. J. Control Release 243, 172–181. https://doi.org/10.1016/j.jconrel.2016.10.007.
Dixon, A.J., et al., 2013. Enhanced intracellular delivery of a model drug using microbubbles produced by a microfluidic device. Ultrasound Med. Biol. 39 (7), 1267–1276. https://doi.org/10.1016/j.ultrasmedbio.2013.01.023.
França, A., , et al.Cerca, N., 2016. Characterization of an in vitro fed-batch model to obtain cells released from S. epidermidis biofilms. AMB Express 6 (1). https://doi.org/10.1186/s13568-016-0197-9.
Gilboa-Garber, N., Sudakevitz, D., 1999. The hemagglutinating activities of Pseudomonas aeruginosa lectins PA-IL and PA-IIL exhibit opposite temperature profiles due to different receptor types. FEMS Immunol. Med. Microbiol. 25 (4), 365–369. https://doi.org/10.1111/j.1574-695X.1999.tb01361.x.
Health, N.I.o., Research on Microbial Biofilms. Report No. PA-03-047. 2002.
Ito, A., et al., 2009. Increased antibiotic resistance of *Escherichia coli* in mature biofilms. Appl Environ Microbiol 75 (12), 4093–4100. https://doi.org/10.1128/AEM.02949-08.
Kinsler, L.E., et al., 2000. Fundamentals of acoustics. John Wiley & Sons.
Klibanov, A.L., et al., 2004. Detection of individual microbubbles of ultrasound contrast agents: imaging of free-floating and targeted bubbles. Invest Radiol 39 (3), 187–195. https://doi.org/10.1097/01.rli.0000115926.96796.75.
Kooiman, K., et al., 2017. Focal areas of increased lipid concentration on the coating of microbubbles during short tone-burst ultrasound insonification. PLoS One 12 (7). https://doi.org/10.1371/journal.pone.0180747 e0180747.
Kooiman, K., et al., 2014. DSPC or DPPC as main shell component influences ligand distribution and binding area of lipid-coated targeted microbubbles. Eur. J. Lipid Sci. Technol. 116 (9), 1217–1227. https://doi.org/10.1002/ejlt.v116.910.1002/ejlt.201300434.
Kooiman, K., et al., 2014. Acoustic behavior of microbubbles and implications for drug delivery. Adv. Drug. Deliv. Rev. 72, 28–48. https://doi.org/10.1016/j.addr.2014.03.003.
Kooiman, K., et al., 2020. Ultrasound-Responsive Cavitation Nuclei for Therapy and Drug Delivery. Ultrasound Med Biol 46 (6), 1296–1325. https://doi.org/10.1016/j.ultrasmedbio.2020.01.002.
Kosareva, A., et al., 2020. Seeing the invisible-ultrasound molecular imaging. Ultrasound. Med. Biol. 46 (3), 479–497. https://doi.org/10.1016/j.ultrasmedbio.2019.11.007.
Kotopoulis, S., et al., 2013. Treatment of human pancreatic cancer using combined ultrasound, microbubbles, and gemcitabine: a clinical case study. Med. Phys. 40 (7), 072902. https://doi.org/10.1118/1.4808149.
Kreitmann, L., et al., 2020. Clinical characteristics and outcome of patients with infective endocarditis diagnosed in a department of internal medicine. J Clin Med 9 (3), 864. https://doi.org/10.3390/jcm9030864.
Kremkau, F.W., 2015. General Principles of Echocardiography. ASE's Compr, Echocardiogr.
Langeveld, S.A.G., et al., 2021. The impact of lipid handling and phase distribution on the acoustic behavior of microbubbles. Pharmaceutics 13 (1), 119. https://doi.org/10.3390/pharmaceutics13010119.
Langeveld, S.A.G., et al., Ligand Distribution and Lipid Phase Behavior in Phospholipid-Coated Microbubbles and Monolayers. Langmuir, 2020. 36(12): p. 3221-3233 DOI: 10.1021/acs.langmuir.9b03912.
Lattwein, K.R., et al., 2020. Sonobactericide: an emerging treatment strategy for bacterial infections. Ultrasound Med. Biol. 46 (2), 193–215. https://doi.org/10.1016/j.ultrasmedbio.2019.09.011.
Lattwein, K.R., et al., 2020. Sonobactericide: an emerging treatment strategy for bacterial infections. Ultrasound. Med. Biol. 46 (2), 193–215. https://doi.org/10.1016/j.ultrasmedbio.2019.09.011.
Lee, S.W., et al., 2021. How microbes read the map: effects of implant topography on bacterial adhesion and biofilm formation. Biomaterials 268, 120595. https://doi.org/10.1016/j.biomaterials.2020.120595.
Lewis, K., 2005. Persister cells and the riddle of biofilm survival. Biochemistry (Mosc) 70 (2), 267–274.
Lipsman, N., et al., 2018. Blood-brain barrier opening in Alzheimer's disease using MR-guided focused ultrasound. Nat. Commun. 9 (1) https://doi.org/10.1038/s41467-018-04529-6.
Lumason Safety Label FDA. Center for Drug Evaluation and Research, Silver Spring, MD, USA 2016.
Lv, K., et al., 2021. Prospective assessment of diagnostic efficacy and safety of SonazoidTM and SonoVue® ultrasound contrast agents in patients with focal liver lesions. Abdominal Radiology 1–13. https://doi.org/10.1109/TIM.2020.3038413.
Mah, T.F., O'Toole, G.A., 2001. Mechanisms of biofilm resistance to antimicrobial agents. Trends Microbiol. 9 (1), 34–39. https://doi.org/10.1016/s0966-842x(00)01913-2.
Mainprize, T., et al., 2019. Blood-brain barrier opening in primary brain tumors with non-invasive MR-guided focused ultrasound: a clinical safety and feasibility study. Sci. Rep. 9 (1) https://doi.org/10.1038/s41598-018-36340-0.
Malek, A.M., Alper, S.L., Izumo, S., 1999. Hemodynamic shear stress and its role in atherosclerosis. JAMA 282 (21), 2035–2042. https://doi.org/10.1001/jama.282.21.2035.
McComas, C.C., Crowley, B.M., Boger, D.L., 2003. Partitioning the loss in vancomycin binding affinity for D-Ala-D-Lac into lost H-bond and repulsive lone pair contributions. J. Am. Chem. Soc. 125 (31), 9314–9315. https://doi.org/10.1021/ja035901x.
Merritt, C.R., Kremkau, F.W., Hobbins, J.C., 1992. Diagnostic ultrasound: bioeffects and safety. Ultrasound. Obstet. Gynecol. 2 (5), 366–374. https://doi.org/10.1046/j.1469-0705.1992.02050366.x.
Mirabel, M., et al., 2014. Long-term outcomes and cardiac surgery in critically ill patients with infective endocarditis. Eur. Heart J. 35 (18), 1195–1204. https://doi.org/10.1093/eurheartj/eht303.
Moccetti, F., et al., 2018. Ultrasound molecular imaging of atherosclerosis using small-peptide targeting ligands against endothelial markers of inflammation and oxidative stress. Ultrasound. Med. Biol. 44 (6), 1155–1163. https://doi.org/10.1016/j.ultrasmedbio.2018.01.001.
Murdoch, D.R., et al., 2009. Clinical presentation, etiology, and outcome of infective endocarditis in the 21st century: the International Collaboration on Endocarditis-Prospective Cohort Study. Arch Int. Med. 169 (5), 463–473. https://doi.org/10.1001/archinternmed.2008.603.
Owen, J., et al., 2019. The role of PEG-40-stearate in the production, morphology, and stability of microbubbles. Langmuir 35 (31), 10014–10024. https://doi.org/10.1021/acs.langmuir.8b02516.
Pritchard, L., et al., 2010. Increasing vancomycin serum trough concentrations and incidence of nephrotoxicity. Am. J. Med. 123 (12), 1143–1149. https://doi.org/10.1016/j.amjmed.2010.07.025.
Rubinstein, E., Keynan, Y., 2014. Vancomycin revisited - 60 years later. Front Public Health 2, 217. https://doi.org/10.3389/fpubh.2014.00217.
Rychak, J.J., Klibanov, A.L., Hossack, J.A., 2005. Acoustic radiation force enhances targeted delivery of ultrasound contrast microbubbles: in vitro verification. IEEE Trans. Ultrason Ferroelectr. Freq. Control 52 (3), 421–433. https://doi.org/10.1109/tuffc.2005.1417264.
Rychak, J.J., et al., 2007. Enhanced targeting of ultrasound contrast agents using acoustic radiation force. Ultrasound. Med. Biol. 33 (7), 1132–1139. https://doi.org/10.1016/j.ultrasmedbio.2007.01.005.
Schinkel, A.F.L., et al., 2020. Contrast-enhanced ultrasound to assess carotid intraplaque neovascularization. Ultrasound. Med. Biol. 46 (3), 466–478. https://doi.org/10.1016/j.ultrasmedbio.2019.10.020.
Sennoga, C.A., et al., 2017. Microbubble-mediated ultrasound drug-delivery and therapeutic monitoring. Expert Opin. Drug. Deliv 14 (9), 1031–1043. https://doi.org/10.1080/17425247.2017.1266328.
Smeenge, M., et al., 2017. First-in-human ultrasound molecular imaging with a VEGFR2-specific ultrasound molecular contrast agent (BR55) in prostate cancer: a safety and feasibility pilot study. Invest. Radiol. 52 (7), 419–427. https://doi.org/10.1097/RLI.0000000000000362.
Stewart, P.S., William Costerton, J., 2001. Antibiotic resistance of bacteria in biofilms. Lancet 358 (9276), 135–138.
Stove, V., et al., Measuring Unbound Versus Total Vancomycin Concentrations in Serum and Plasma: Methodological Issues and Relevance. Therapeutic Drug Monitoring, 2015. 37(2).
Tahon, J., et al., 2021. Long-term follow-up of patients with infective endocarditis in a tertiary referral center. Int. J. Cardiol. 331, 176–182. https://doi.org/10.1016/j.ijcard.2021.01.048.
Takalkar, A.M., et al., 2004. Binding and detachment dynamics of microbubbles targeted to P-selectin under controlled shear flow. J. Control Release 96 (3), 473–482. https://doi.org/10.1016/j.jconrel.2004.03.002.
Tongsai, S., Koomanachai, P., 2016. The safety and efficacy of high versus low vancomycin trough levels in the treatment of patients with infections caused by methicillin-resistant Staphylococcus aureus: a meta-analysis. BMC Res Notes 9 (1), 455. https://doi.org/10.1186/s13104-016-2252-7.
Unnikrishnan, S., et al., 2019. Formation of microbubbles for targeted ultrasound contrast imaging: practical translation considerations. Langmuir 35 (31), 10034–10041. https://doi.org/10.1021/acs.langmuir.8b03551.
van der Meer, S.M., et al., 2007. Microbubble spectroscopy of ultrasound contrast agents. J. Acoust. Soc. Am. 121 (1), 648–656. https://doi.org/10.1121/1.2390673.
van Oosten, M., et al., 2013. Real-time in vivo imaging of invasive- and biomaterial-associated bacterial infections using fluorescently labelled vancomycin. Nat. Commun. 4 (1) https://doi.org/10.1038/ncomms3584.
van Rooij, T., et al., 2015. Targeted ultrasound contrast agents for ultrasound molecular imaging and therapy. Int. J. Hyperthermia 31 (2), 90–106. https://doi.org/10.3109/02656736.2014.997809.

van Rooij, T., et al., 2016. Viability of endothelial cells after ultrasound-mediated sonoporation: Influence of targeting, oscillation, and displacement of microbubbles. J. Controlled Release: Off. J. Controlled Release Soc. 238, 197–211. https://doi.org/10.1016/j.jconrel.2016.07.037.

Wang, S., et al., 2016. Ultra-Low-Dose Ultrasound Molecular Imaging for the Detection of Angiogenesis in a Mouse Murine Tumor Model: How Little Can We See? Invest. Radiol. 51 (12), 758–766. https://doi.org/10.1097/RLI.0000000000000310.

Wang, F., et al., 2018. Insights into Key interactions between vancomycin and bacterial cell wall structures. ACS Omega 3 (1), 37–45. https://doi.org/10.1021/acsomega.7b01483.

Waters, E.M., et al., 2016. Convergence of staphylococcus aureus persister and biofilm research: can biofilms be defined as communities of adherent persister cells? PLoS Pathog 12 (12), e1006012. https://doi.org/10.1371/journal.ppat.100601210.1371/journal.ppat.1006012.g001.

Wille, J., Coenye, T., 2020. Biofilm dispersion: The key to biofilm eradication or opening Pandora's box? Biofilm 2, 100027. https://doi.org/10.1016/j.bioflm.2020.100027.

Willmann, J.K., et al., 2017. Ultrasound molecular imaging with BR55 in patients with breast and ovarian lesions: first-in-human results. J. Clin. Oncol. 35 (19), 2133–2140. https://doi.org/10.1200/JCO.2016.70.8594.

Xing, Z., et al., 2010. Novel ultrasound contrast agent based on microbubbles generated from surfactant mixtures of Span 60 and polyoxyethylene 40 stearate. Acta Biomater. 6 (9), 3542–3549. https://doi.org/10.1016/j.actbio.2010.03.007.